SMALL-SIZE UNMANNED MODEL HELICOPTER GUIDANCE AND CONTROL

A THESIS SUBMITTED TO
THE GRADUATE SCHOOL OF NATURAL AND APPLIED SCIENCES
OF
MIDDLE EAST TECHNICAL UNIVERSITY

BY

ÇAĞLAR KARASU

IN PARTIAL FULFILLMENT OF THE REQUIREMENTS FOR

THE DEGREE OF MASTER OF SCIENCE
IN
ELECTRICAL AND ELECTRONICS ENGINEERING

NOVEMBER 2004

Approval of the Graduate School of Natural and Applied Sciences

_____

Prof. Dr. Canan Özgen
Director

I certify that this thesis satisfies all the requirements as a thesis for the degree of Master of Science.

_____

Prof. Dr. İsmet Erkmen
Head of Department

This is to certify that we have read this thesis and that in our opinion it is fully adequate, in scope and quality, as a thesis for the degree of Master of Science.

_____

Prof. Dr. Kemal Leblebicioğlu
Supervisor

Examining Committee Members

Prof. Dr. Erol Kocaoğlan (METU, EE) _____

Prof. Dr. Kemal Leblebicioğlu (METU, EE) _____

Prof. Dr. Kemal Özgören (METU, ME) _____

Prof. Dr. Uğur Halıcı (METU, EE) _____

Dr. Burak Kaygısız (TUBITAK-SAGE) _____

I hereby declare that all information in this document has been obtained and presented in accordance with academic rules and ethical conduct. I also declare that, as required by these rules and conduct, I have fully cited and referenced all material and results that are not original to this work.

Çağlar KARASU

ABSTRACT

SMALL-SIZE UNMANNED MODEL HELICOPTER GUIDANCE AND CONTROL

Karasu, Çağlar

M.S., Department of Electrical and Electronics Engineering

Supervisor: Prof. Dr. Kemal Leblebicioğlu

November 2004, 93 Pages

The deployment of unmanned aerial vehicles (UAV) in military applications increased the research about them and the importance of them. The unmanned helicopters are the most agile and maneuverable vehicles among the unmanned aerial vehicles (UAV). The ability of hovering and low speed cruise makes them even more attractive. Such abilities supply more areas to deploy the usage of the unmanned helicopters like search & rescue, mapping, surveillance. Autonomy is the key property for these vehicles. In order to provide autonomy to an unmanned vehicle, the guidance and the autopilot units are designed in the first step. Waypoints are used to track the desired trajectories. The line of sight guidance is used to reach an active waypoint. In order to realize the guidance commands controllers are designed by using LQR. In addition, position and heading controllers are designed by root-locus method. The trimming and linearization are implemented in order to extract linear models used for controller design.

Keywords: Helicopter, control, guidance

ÖZ

KÜÇÜK BOYUTLU İNSANSIZ MODEL HELİKOPTER DENETİM VE GÜDÜMÜ

Karasu, Çağlar

Yüksek Lisans, Elektrik ve Elektronik Mühendisliği Bölümü

Tez Yöneticisi: Prof. Dr. Kemal Leblebicioğlu

Kasım 2004, 93 Sayfa

İnsansız hava araçlarının askeri alanlarda kullanılmasıyla bu konudaki araştımalar ve bu konunun önemi artmıştır. İnsansız helikopterler, insansız hava araçları içersinde en atik ve manevra kabiliyeti en yüksek olan araçlardır. Havada asılı kalmaları ve yavaş hareket edebilmeleri helikopterlere olan ilgiyi arttırmaktadır. Bu tür kabiliyetleri insansız helikopterlerin arama ve kurtarma, gözetim ve haritacılık gibi çeşitli alanlarda kullanılmasına olanak tanımaktadır. Otonom özelliği bu tür uygulamalar için anahtardır. Bu araçlara otonom özellik kazandırılması için tasarlanması gerekenler arasında güdüm ve denetim algoritmaları temel olanlarıdır. Yol noktaları istenen rotanın takip edilebilmesi için kullanılmıştır. LOS güdüm yöntemi kullanılarak helikopter yol noktalarına ulaştırılmıştır. Güdüm komutlarının gerçekleştirilmesi için LQR yöntemiyle bir denetimci tasarlanmıştır. Ayrıca, konum denetimcileri de helikopterin havada asılı kalabilmesi için root-locus yöntemiyle tasarlanmıştır. Denetimci tasarımı için doğrusal olmayan model doğrusallaştırılmıştır ve denge durumları bulunmuştur.

Keywords: Helikopter, denetim, güdüm

ACKNOWLEDGEMENTS

I would like to express my appreciation to my supervisor Prof. Dr. Kemal Leblebicioğlu for his support and advices during my research.

I want to thank Burak Kaygısız for his guidance throughout my work. His support and assistance was invaluable to me. In addition, I want to thank my friends in TUBİTAK-SAGE for their encouragements and for their last long patience, especially to Kadriye Tiryaki and Ahmet E. Güçiz.

I am vey grateful to Alper Unver and Yüksel Subaşı for their support and encouragement during this study especially in the dark days.

I also thank to my fellows Mustafa İspir, Abdullah G. Gençay and Tuba Bayık for their enjoyable friendship.

I want to thank my friends Ekin Dino, Yağız Yaşaroğlu, Özgür Önür and Medeni Soysal for their patience.

TUBİTAK-SAGE, which supported this work, is acknowledged.

Finally, I want to thank my family for their consistent support.

TABLE OF CONTENTS

LIST OF FIGURES

FIGURES

CHAPTER 1

INTRODUCTION

Aerial vehicles are used in military and civilian applications very widely. Among them, the most agile and maneuverable ones are the helicopters. Their low speed cruise and hover capability enables them to track the desired trajectories very precisely. These advantages make them superior than the fixed-wing aircrafts. However, control of a helicopter is much more difficult to achieve than control of a fixed-wing aircraft.

The unmanned small helicopters are much more attractive than the full-size helicopters. The cost effective and safe way to protect the pilots from the dangerous situations is the use of autonomous unmanned vehicles instead of the piloted air vehicles. In fact, the UAVs have proven to be effective for military reconnaissance missions at the front line [19]. In addition, they are already exploited in civil life such as agricultural applications but not autonomously. Moreover, they are very promising in infrastructure maintenance and environmental issues. To accomplish such missions autonomously, unmanned vehicles have to acquire some level of autonomy. The autonomy depends on the utilization of guidance and the high-level decision making algorithms. The high-level management systems are the ongoing research topic. The route planners, obstacle avoidance techniques, failure management systems are these kind of topics [20].

The autopilot and guidance techniques are the first steps of the flight management systems. There are several difficulties of designing autopilots for small-size unmanned helicopters. The autopilot designs mostly based on the mathematical model of the helicopter. Since the nature of these aerial vehicles is very complex, the accurate models for large portion of the flight envelope are difficult to collect.

However, some techniques have been developed. First principles modeling and system identification are the different but the complementary techniques. By the first principles techniques, the linear models at trim points are produced. The main drawback of this technique is the requirement of the many physical parameters. The system identification technique based on the time response data or the frequency-response data from the flight tests. The main problem of the system identification is the difficulty of simulating the full envelope. By combining these two techniques, accurate models are generated for the flight control systems.

The most common control design approach for autonomous helicopters is two-loop design. First, an inner loop that provides high performance tracking of attitude commands is design, subsequent to which an outer loop that tracks translational variables is designed [15]. There are researchers who used H_∞ [2], neural-based adaptive [21] and fuzzy logic methods to design flight control systems.

1.1 Scope of the Thesis

This study is about designing an autopilot for a small-size unmanned helicopter. In addition, waypoint guidance algorithm is implemented in order to track a desired trajectory.

1.2 Thesis Outline

Chapter 2: This chapter presents a mathematical model for a model-scale unmanned helicopter. The governing equations of motion are derived by applying Newton's laws of motion, which relate the summation of the external forces and moments. The external force and moments due to aerodynamic and thrust are detailed in this chapter.

Chapter 3: In trajectory tracking, a priori known flight path is desired to be tracked by the helicopter. Thus, the generation of the desired path is implemented. After the generation of a trajectory, an optimization algorithm calculates the control inputs in order to minimize the error between the desired trajectory and the actual trajectory.

Chapter 4: In this chapter, the trimming and the linearization are introduced in order to design a linear controller. Trim points are determined by an iterative algorithm with prescribed variables. Linearization is implemented by numerical and analytical differentiation.

Chapter 5: The autopilot design is presented in chapter 5. The LQR method is used to implement the controller design. Two decoupled autopilots are implemented. The local linear controllers are designed at the various trim points, which cover the flight envelope. The local linear controllers are used to attain global controller by using gain scheduling.

Chapter 6: Waypoint guidance is used for the guidance method in this chapter. A sequence of waypoints is used for tracking a path. The active waypoint is used by the guidance algorithm as the target position. The next waypoint is activated when the previous waypoint is reached and the sequence will end up with a trajectory

Chapter 7: Conclusions are given in this chapter.

CHAPTER 2

MATHEMATICAL MODELING

This chapter presents a mathematical model for a model-scale unmanned helicopter. The mathematical model is essential for designing control laws and for simulation. The flight controllers are based on the dynamic models. Reliable controllers can be designed by using accurate models for a large flight envelope. For constructing dynamic models, linear system identification methods are used. The linear system identification shows that the dynamics of small size helicopter governed by the first order effects [14]. However, the linear models extracted from linear system identification are valid around an operating point. Accurate nonlinear models are constructed by using flight test data for large flight envelope. The model used in this study is based on an experimental helicopter used in [4].

In this chapter, the coordinate systems and the equations of motion are presented. The coordinate systems are used for description of the motion of the helicopter. The governing equations of motion are derived by applying Newton's laws of motion, which relate the summation of the external forces and moments to the rate of changes of positions and velocities. The external force and moments due to aerodynamic and thrust are detailed.

2.1 Coordinate Systems and Frames

To develop the equations of motion, there should be a non-rotating and non-accelerating frame for which the Newton's Laws are valid. This frame is called inertial reference frame. However, there is not any non-rotating and non-accelerating frame. The motion of the Earth is negligible, if the velocity of the body is small and the time of flight is short. In addition, the equations of motion will be

simplfied by taking the Earth as flat. In this thesis, the inertial frame is taken as the Earth-fixed reference frame and the equations are the flat-earth frame equations.

Earth-fixed reference frame is taken to be fixed to the Earth's surface with its X axis pointing towards north, Y axis pointing towards east and Z axis pointing towards down to the centre of the earth.

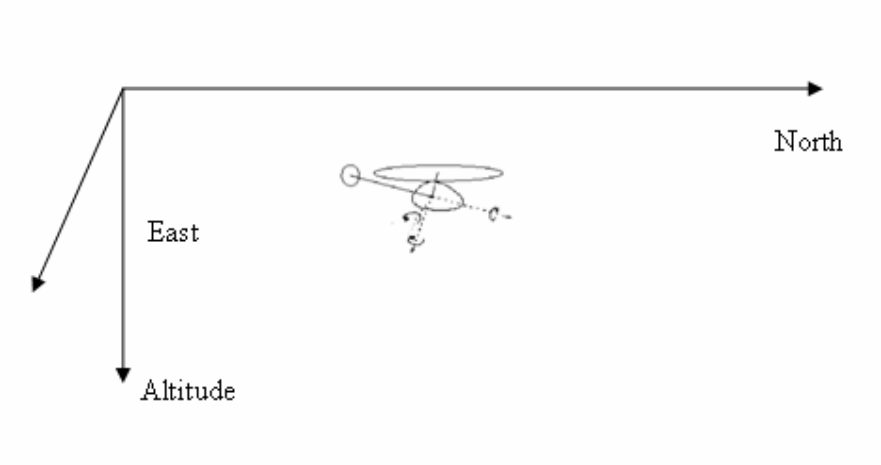

Figure 2-1 Earth-fixed reference frame and body-fixed frame

It is appropriate to express the forces and velocities in an orthogonal-body coordinate frame (body-fixed frame). This frame is centered at the center of gravity of the ridig body and its x axis points from the center of gravity to the nose of the body, y axis points toward right of the body looking from the rear, z axis points down, forming a right handed orthogonal coordinate system.

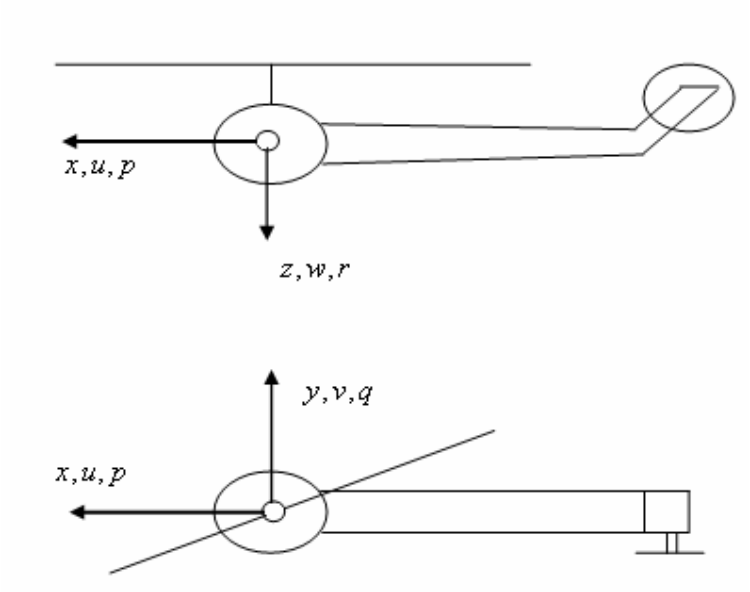

Figure 2-2 Body-fixed frame

Any vector in the earth-fixed reference frame can be transformed to the body-fixed frame by the linear transformation as in Eq. (2-1)

$$X_B = C_E^B X_E \tag{2-1}$$

The transformation matrix C_E^B is called the direction cosine matrix. This transformation matrix is an orthonormal matrix and describes the orientation of body-fixed frame with respect to the earth-fixed reference frame. Also the orientation of three-dimensional coordinate frame w.r.t another can be described by a sequence of basic rotation matrices. These rotations are

- Rotation about the z-axis (yaw Ψ)
- Rotation about the new y-axis (pitch θ)
- Rotation about the new x-axis (roll ϕ)

The yaw, pitch, and the roll angles are commonly known as Euler angles. The basic rotation matrices are expressed as follows:

$$C_1 = \begin{bmatrix} \cos(\Psi) & -\sin(\Psi) & 0 \\ \sin(\Psi) & \cos(\Psi) & 0 \\ 0 & 0 & 1 \end{bmatrix} \tag{2-2}$$

$$C_2 = \begin{bmatrix} \cos(\theta) & 0 & \sin(\theta) \\ 0 & 1 & 0 \\ -\sin(\theta) & 0 & \cos(\theta) \end{bmatrix} \tag{2-3}$$

$$C_3 = \begin{bmatrix} 1 & 0 & 0 \\ 0 & \cos(\phi) & -\sin(\phi) \\ 0 & \sin(\phi) & \cos(\phi) \end{bmatrix} \tag{2-4}$$

The complete transformation can be written as in Eq. (2-5) by taking the products of the basic rotations in Eq. (2-2),(2-3),(2-4)

$$C_E^B = \begin{bmatrix} c\theta c\Psi & c\theta s\Psi & -s\theta \\ -c\Phi s\Psi + s\Phi s\theta s\Psi & c\Phi c\Psi + s\Phi s\theta s\Psi & s\Phi c\theta \\ s\Phi s\Psi + c\Phi s\theta c\Psi & -s\Phi c\Psi + c\Phi s\theta s\Psi & c\Phi c\theta \end{bmatrix} \tag{2-5}$$

where c's stand for cosinus and s's stand for sinus.

2.2 Dynamic Equations of Motion

It is assumed that the helicopter is rigid body. Therefore, the distance between any two points on the helicopter does not change during flight.

A rigid body can simultaneously have two kinds of motion: it can change its position in space and it can change its orientation in space. So, any rigid body can be considered to have six degrees of freedom.

Translational Dynamics

Change in position is translational motion. This can be described by the motion of the center of mass. From Newton's second Law it can be deduced that

$$\vec{F} = \frac{d}{dt}(m\vec{V}_T) \tag{2-6}$$

where $\vec{F}$ is the total external force applied to the body and $\vec{V}_T$ is the total velocity of the body. The derivative of total velocity $\vec{V}_T$ w.r.t Earth-fixed reference frame is composed of the derivative of total velocity w.r.t body-fixed frame and the cross product of the angular velocity of the body and the total velocity. This second term is known as the Coriolis Effect.

$$\frac{d}{dt}(\vec{V}_T)_E = (\frac{d}{dt}\vec{V}_T)_B + \vec{\omega} \times \vec{V}_T \tag{2-7}$$

The need for the coriolis equation arises when there are two or frames rotating relative to each other. The Coriolis Effect is the motion resulting from the relative angular velocity of the moving frame with respect to the reference frame. The vectors are expressed in the body-fixed frame as

$$\vec{V}_T = \vec{i}\,u + \vec{j}v + \vec{k}w \tag{2-8}$$

$$\vec{\omega} = \vec{i}\,p + \vec{j}q + \vec{k}r \tag{2-9}$$

where $\vec{i}$, $\vec{j}$, and $\vec{k}$ are the unit vectors along the body-fixed frame axes x, y, z respectively. The force $\vec{F}$ in Eq. (2-6) can be expressed as in Eq. (2-10) by using Eqns. (2-7), (2-8) and (2-9).

$$\vec{F} = m\left\{(\dot{u} + qw - vr)\vec{i} + (\dot{v} + ur - pw)\vec{j} + (\dot{w} + pv - uq)\vec{k}\right\} \tag{2-10}$$

The force $\vec{F}$ can be expressed in body-fixed frame as in Eq.(2-11)

$$\vec{F} = \vec{i}F_x + \vec{j}F_y + \vec{k}F_z \tag{2-11}$$

where F_x, F_y, F_z are the components of the total force acting on the body expressed in the body-fixed frame. The translational equations are found by combining the Eqns. (2-10) and (2-11) as

$$\dot{u} = vr - qw + \frac{F_x}{m} \tag{2-12}$$

$$\dot{v} = pw - ur + \frac{F_y}{m} \tag{2-13}$$

$$\dot{w} = uq - pv + \frac{F_z}{m} \tag{2-14}$$

Rotational Dynamics

Change in orientation is rotational motion. This motion can be regarded as a rotation about some axis. The acting torques can be written by the Newton's second law as

$$\vec{M} = \frac{d}{dt}(\vec{H}) \tag{2-15}$$

where $\vec{M}$ is the total torques applied to the body, and the $\vec{H}$ is angular momentum. Angular momentum is defined as

$$\vec{H} = I\vec{\omega} \tag{2-16}$$

where I is the inertia matrix and $\vec{\omega}$ is the angular velocity. The inertia matrix is defined as

$$I = \begin{bmatrix} I_{xx} & -I_{xy} & -I_{xz} \\ -I_{xy} & I_{yy} & -I_{yx} \\ -I_{xz} & -I_{yz} & I_{zz} \end{bmatrix} \tag{2-17}$$

The components of this inertia matrix are the moments of inertia. Moment of inertia is a measure of the resistance that a body offers to changes in its rotational motion just as mass is a measure of resistance that a body offers to change its translational motion. The moment of inertia depends on the location of the axis of rotation. The moment of inertia is small if the axis passes through the center of mass. I_{xy}, I_{xz}, I_{yz} are the product of inertia terms, and taken to be the zero if the body is symmetric. In this thesis, the helicopter body is taken as symmetric hence the cross product of inertia terms are zero.

$$\frac{d}{dt}(\vec{H})_E = \frac{d}{dt}(\vec{H})_B + \vec{\omega} \times \vec{H} \tag{2-18}$$

The moment equation in the body-fixed frame becomes as in Eq. (2-19) by combining Eqns. (2-16), (2-17), (2-18) and the Eq. (2-9).

$$\vec{M} = (\dot{p}I_{xx} + qr(I_{zz} - I_{yy}))\vec{i} + (\dot{q}I_{yy} + pr(I_{xx} - I_{zz}))\vec{j} + (\dot{r}I_{zz} + pq(I_{yy} - I_{xx}))\vec{k} \tag{2-19}$$

The moment $\vec{M}$ can be expressed in body-fixed frame as in Eq. (2-20)

$$\vec{M} = \vec{i}M_x + \vec{j}M_y + \vec{k}M_z \tag{2-20}$$

where M_x, M_y, M_z are the components of the total moment acting on the body about its mass center expressed in the body frame. The rotational dynamics are found by combining the Eqns. (2-19) and (2-20)

$$\dot{p} = qr(I_{yy} - I_{zz})/I_{xx} + M_x/I_{xx} \tag{2-21}$$

$$\dot{q} = pr(I_{zz} - I_{xx})/I_{yy} + M_y/I_{yy} \tag{2-22}$$

$$\dot{r} = pq(I_{xx} - I_{yy})/I_{zz} + M_z/I_{zz} \tag{2-23}$$

2.3 Kinematic Dynamics

In order to describe the motion of the body w.r.t the earth-fixed reference frame, it is necessary to specify the orientation of body-fixed frame with respect to Earth-fixed reference frame. The orientation is the physical relationship that depends on two frames. In order to derive this geometric relationship during the flight, there are kinematic differential equations of motion.

Translational Kinematics

The relation between the velocities in earth-fixed reference frame and body-fixed frame is given by:

$$\frac{d}{dt}\begin{bmatrix} X \\ Y \\ Z \end{bmatrix} = C_B^E \begin{bmatrix} u \\ v \\ w \end{bmatrix} \tag{2-24}$$

where X , Y , Z are the position of the body w.r.t earth-fixed reference frame, and u , v , w are the velocities of the body w.r.t body frame. C_B^E is the transformation matrix from the body-fixed frame to the earth-fixed reference frame.

Rotational Kinematics

Rotational kinematic equations are the differential equations of the Euler angles. The Euler angles change by angular velocities of the body. By using the orthonormal property of the direction cosine matrix and the differentiation of vectors, one can find the rotational kinematics.

Let V_B be a vector defined in the body-fixed frame and V_E be a vector defined in the earth-fixed reference frame. Suppose C_E^B is the transformation matrix from earth-fixed reference frame to the body-fixed frame.

$$
\begin{aligned}
&\vec{V}_B = C_E^B \vec{V}_E \\
&\frac{d}{dt_E}\vec{V}_B = C_E^B \dot{\vec{V}}_E \\
&\frac{d}{dt_B}\dot{\vec{V}}_B = \dot{\vec{V}}_B = C_E^B \dot{\vec{V}}_E + (\dot{C}_E^B) V_E \\
&\frac{d}{dt_E}\dot{\vec{V}}_B = \dot{\vec{V}}_B - \dot{C}_E^B \vec{V}_E
\end{aligned}
\tag{2-25}
$$

The transformation between Earth-fixed reference frame and the body-fixed frame is shown in the first line of the Eq (2-25). The derivative of V_B with respect to the Earth frame is shown in the second line of Eq (2-25). In the third line of Eq (2-25), the derivative of the V_B with respect to the body-fixed frame is shown.

The Coriolis Effect in the Eq (2-7) can be written as

$$
\vec{\omega}_B \times \vec{V}_B = \Omega_B C_E^B \vec{V}_E \tag{2-26}
$$

where Ω_B is the cross-product matrix for the cross-product operation and $\omega_B = \begin{bmatrix} p & q & r \end{bmatrix}^T$.

$$
\Omega_B = \begin{bmatrix} 0 & -r & q \\ r & 0 & -p \\ -q & p & 0 \end{bmatrix} \tag{2-27}
$$

The Eq. (2-28) is written by equating Eq. (2-26) and Eq. (2-25).

$$
\begin{aligned}
&\dot{C}_E^B = -\Omega_B C_E^B \\
&\Omega_B = \dot{C}_E^B C_E^B
\end{aligned}
\tag{2-28}
$$

The rotational kinematic equations are found as

$$
\dot{\phi} = p + \tan(\theta)(q\sin(\phi) + r\cos(\phi)) \tag{2-29}
$$

$$\dot{\theta} = q\cos(\phi) - r\sin(\phi) \tag{2-30}$$

$$\dot{\psi} = (q\sin(\phi) + r\cos(\phi))\sec(\theta) \tag{2-31}$$

2.4 Helicopter Aerodynamics

The helicopter has the ability to fly at low speed and to hover. The low speed performance of the helicopter enables to follow the precise trajectories. These capabilities are because of the continuously rotating blades attached to the rotor. The circular plane that the blades sweep through is called rotor disc. The blades have the property of an airfoil that generates lift by pushing the air down. At the same time, the blade receives a resisting torque in the opposite direction of the rotor revolution, which is transmitted to the fuselage and causes spin in the opposite direction of the rotor revolution [20]. This torque is called anti-torque and cancelled by the tail rotor. The tail rotor is mounted at end of the fuselage and the shaft of the rotor is along the y axis of the body axis frame.

A helicopter can be modeled as a combination of five subsystems. These are the main rotor, tail rotor, fuselage, empennage and engine. The empennage is composed of vertical fins and the horizontal stabilizers. They are shown in Figure 2-3. The forces and moments produced by these subsystems are shown in dynamic equations derived in the previous section in Eq. (2-32) where mr represents for the main rotor, fus for fuselage, tr for tail rotor, vf for vertical fin and ht for the horizontal stabilizer

$$\begin{aligned}
\dot{u} &= vr - wq - g\sin\theta + (X_{mr} + X_{fus})/m \\
\dot{v} &= wp - ur + g\sin(\Phi)\cos(\theta) + (Y_{mr} + Y_{fus} + Y_{tr} + Y_{vf})/m \\
\dot{w} &= uq - vp + g\cos(\Phi)\cos(\theta) + (Z_{mr} + Z_{fus} + Z_{ht})/m \\
\dot{p} &= qr(I_{zz} - I_{yy})/I_{xx} + (L_{mr} + L_{vf} + L_{tr})/I_{xx} \\
\dot{q} &= pr(I_{xx} - I_{zz})/I_{yy} + (M_{mr} + M_{ht})/I_{yy} \\
\dot{r} &= pq(I_{yy} - I_{xx})/I_{zz} + (-Q_e + N_{vf} + N_{tr})/I_{zz}
\end{aligned} \tag{2-32}$$

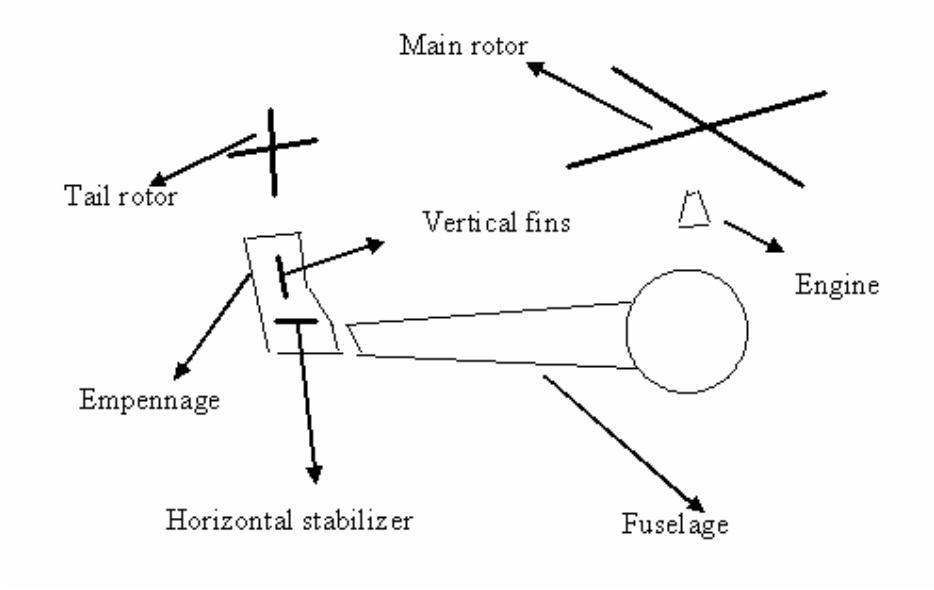

Figure 2-3 Helicopter subsystems

The basic control is to change the magnitude and direction of the thrust produced by the main rotor. The magnitude of the thrust is controlled by collectively altering the pitch angles of all the blades together. This collective pitch displacement is denoted as θ_0 shown in Figure 2-4.

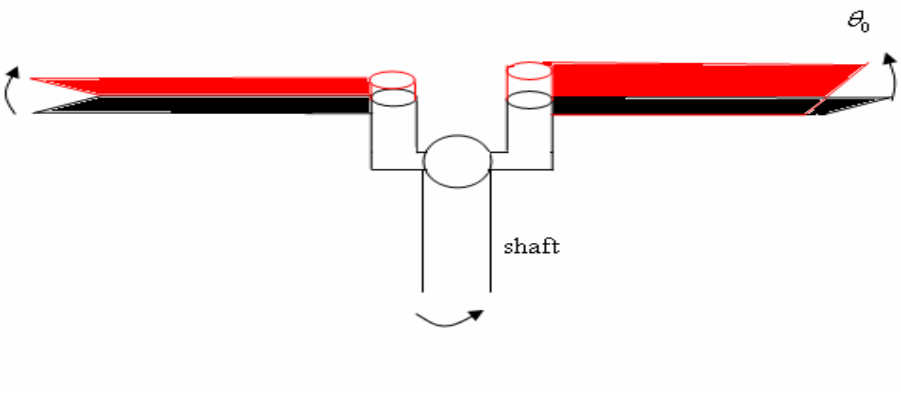

Figure 2-4 Collective control angle

The direction of the thrust can be changed by using cyclic inputs. By cyclic inputs, the flap angle of the blade is controlled. The flap angle is shown in Figure 2-5 determines the direction of the thrust w.r.t the fuselage. By longitudinal cyclic input δ_{lon}, the blade traveling toward to the front of the helicopter flaps down. The blade traveling toward to the back of the helicopter flaps up. Thus, the direction of the thrust of the main rotor is directed forward. The lateral cyclic input δ_{lat} directs the thrust sideways in a similar fashion.

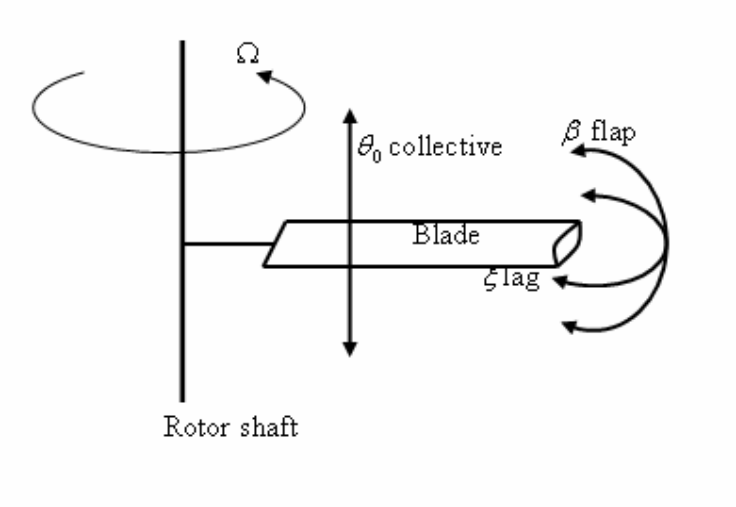

Figure 2-5 Fundamental blade motion [3]

The tail rotor control is provided by only collective pitch denoted as δ_{tail}. The main rotor torque is compensated by tail rotor thrust. Heading of the helicopter can also be directed by tail rotor while the helicopter hovers.

In order to design controllers for the small-size helicopter for a large portion of the flight envelope, there should be accurate models. The helicopter body is connected to several elastic bodies such as rotor and control surfaces. Moreover, the nonlinear aerodynamic forces and gravity act on the vehicle. Hence, the analysis is difficult. There are some assumptions to overcome complexity problems. The assumptions used in this thesis are

- The aircraft can be treated as a rigid body with any number of spinning rotors,
- There is a plane of symmetry, so that $I_{xy}=I_{yz}=0$,
- The axes of spinning rotors are fixed in the direction relative to the body axes and have constant angular speed relative to the body axes,
- Inflow is steady and uniform.

2.4.1 Main Rotor Thrust & Torque

The forces and moments produced by the subsystems of helicopter are shown in Eq. (2-32). The main rotor thrust is the key component in the force and moment calculations. The momentum theory treats the rotor as an actuator disk with zero thickness and circular surface, able to support a pressure difference and thus accelerate air through the disk [3]. The resulting airflow is called induced inflow and sometimes it is called downwash velocity.

The thrust coefficient is used to calculate the thrust provided by the main rotor

$$C_T = \frac{T}{\rho(\Omega R)^2 \pi R^2} \tag{2-33}$$

where C_T is the thrust coefficient and the R is the radius of the main rotor blade and T is the thrust. The iterative scheme based on momentum theory given by Padfield [1] is used to compute the thrust coefficient. The following equations can be solved iteratively.

$$\lambda_0 = \frac{C_T}{2\eta_w \sqrt{\mu^2 + (\lambda_0 - \mu_z)^2}}$$

$$C_T^{ideal} = \frac{a\sigma}{2}(\theta_0(\frac{1}{3} + \frac{\mu^2}{2}) + \frac{\mu_z - \lambda_0}{2})$$

$$C_T = \begin{cases} C_T^{ideal} & if \quad -C_T^{\max} \le C_T^{ideal} \le C_T^{\max} \\ -C_T^{\max} & if \quad C_T^{ideal} < -C_T^{\max} \\ C_T^{\max} & if \quad C_T^{\max} < C_T^{ideal} \end{cases} \qquad (2\text{-}34)$$

$$C_T^{\max} = \frac{T^{\max}}{\rho(\Omega R)^2 \pi R^2}$$

Here

$$\mu = \frac{\sqrt{(u - u_{wind})^2 + (v - v_{wind})^2}}{\Omega R} - advance \quad ratio$$

$$\mu_z = \frac{w - w_{wind}}{\Omega R} - normal \quad airflow \quad component$$

$$\sigma = \frac{2c}{\pi R} - solidity \quad ratio$$

$$a - lift \quad curve \quad slope \qquad (2\text{-}35)$$

$$\theta_0 - commanded \quad collective \quad angle$$

$$\eta_w - coefficient \quad of \; non - ideal \quad wake \quad contraction$$

$$T^{\max} - \max imum \quad rotor \quad thrust$$

A coefficient, η_w is introduced for the non-uniform flow. This coefficient is approximated as 0.9 by [4]. The iterative scheme given in [4] is

$$g_0 = \lambda_0 - \frac{C_T}{2\eta_w \Lambda^{1/2}} \qquad (2\text{-}36)$$

$$\Lambda = \mu^2 + (\lambda_0 - \mu_z)^2$$

where the thrust coeffiecient C_T is given by Eq. (2-34). Applying Newton's iterative scheme we obtain the following.

$$\lambda_{0_{j+1}} = \lambda_{0_j} + f_i h_j(\lambda_{0_j})$$
$$h_j = -\left(\frac{g_0}{dg_0/d\lambda_0}\right)_{\lambda_0=\lambda_{0_j}} \tag{2-37}$$

An explicit expression for h_j is

$$h_j = -\frac{\left(2\eta_w \lambda_{0_j} \Lambda^{1/2} - C_T\right)\Lambda}{2\eta_w \Lambda^{3/2} + \frac{a\sigma}{4}\Lambda - C_T(\mu_z - \lambda_{0_j})} \tag{2-38}$$

Padfield suggests a constant value of the convergence rate coefficient $f_i = 0.6$. This scheme is used to compute the the thrust coefficient of the main rotor at every integration time of the simulation since the thrust coefficient depends on the collective control input, inflow and the velocity of the helicopter. Then the thrust is computed as

$$T = C_T \rho(\Omega R)^2 \pi R^2 \tag{2-39}$$

In order to compute the body-fixed frame velocities using Newton's laws, the main rotor force components should be projected to the body-fixed axes. The rotor thrust taken as perpendicular to the tip-path plane shown in Figure 2-7 while advance ratio ($\mu < 0.15$) is small. The linear relation for the transformation is valid since the flap angles of the blades are small.

$$X_{mr} = -Ta_1$$
$$Y_{mr} = Tb_1 \tag{2-40}$$
$$Z_{mr} = -T$$

The main rotor torque can be determined after the computation of the thrust coefficient. The main rotor torque can be approximated as a sum of induced torque due to generated thrust, and torque due to profile drag on the blades [1].

$$C_Q = \frac{Q}{\rho(\Omega R)^2 \pi R^3} = C_T(\lambda_0 - \mu_z) + \frac{c_{D_0}\sigma}{8}(1 + \frac{7}{3}\mu^2) \quad (2\text{-}41)$$

where C_Q is the torque coefficient, C_{D_0} is the profile drag coefficient of the main rotor blade. The torque is

$$Q_{mr} = C_Q \rho(\Omega R)^2 \pi R^3 \quad (2\text{-}42)$$

2.4.2 Main Rotor Moments

The main rotor moments are produced mainly because of flapping of the blades. The degrees of freedom of the rotor blades are the flap, lag and the torsional motion. The angles corresponding to these motions are the β, ξ, and θ_0 shown in Figure 2-6. The direction of the main rotor thrust is determined by the flap angle.

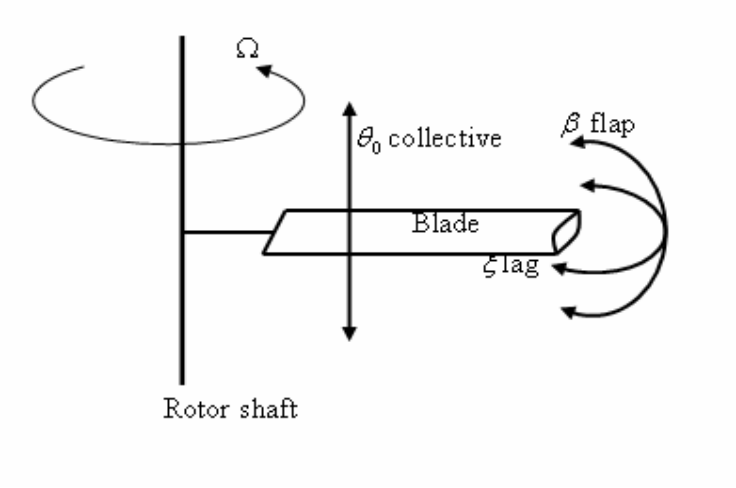

Figure 2-6 Fundamental blade motion [3]

The steady-state blade motion is periodic around the azimuth. Using the Fourier series expansion, the flap motion is written as

$$\beta(t) = a_0(t) - a_1(t)\cos(\Psi) + b_1(t)\sin(\Psi) \quad (2\text{-}43)$$

where $a_0(t)$ is coning angle, $a_1(t)$, and $b_1(t)$ represents the pitching and the rolling motion of the tip-path plane (TPP) [3].

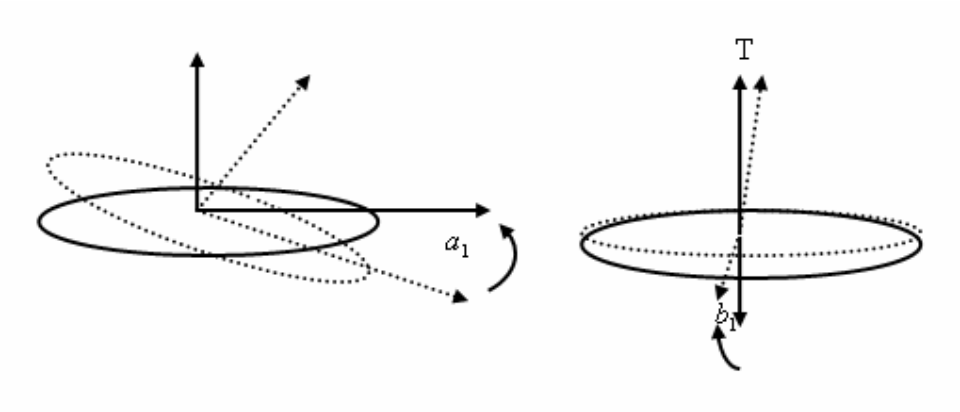

Figure 2-7 Tip path plane

The flapping dynamics are presented as [4]

$$\begin{aligned}\dot{b}_1 &= -p - \frac{b_1}{\tau_e} - \frac{1}{\tau_e}\frac{\partial b_1}{\partial \mu_v}\frac{v - v_{wind}}{\Omega R} + \frac{B_{\delta_{lat}}}{\tau_e}\delta_{lat} \\ \dot{a}_1 &= -q - \frac{a_1}{\tau_e} - \frac{1}{\tau_e}\left(\frac{\partial a_1}{\partial \mu}\frac{u - u_{wind}}{\Omega R} + \frac{\partial a_1}{\partial \mu_z}\frac{w - w_{wind}}{\Omega R}\right) + \frac{A_{\delta_{lon}}}{\tau_e}\delta_{lon}\end{aligned} \tag{2-44}$$

where $B_{\delta_{lat}}$, $A_{\delta_{lon}}$ are the effective steady-state lateral and longitudinal gains from the cyclic inputs to the main rotor flap angles. δ_{lat}, δ_{lon} are the lateral and the longitudinal control inputs. u_{wind}, v_{wind} and w_{wind} are the wind components along the X, Y, and Z helicopter body axes. τ_e is the effective rotor time constant [4].

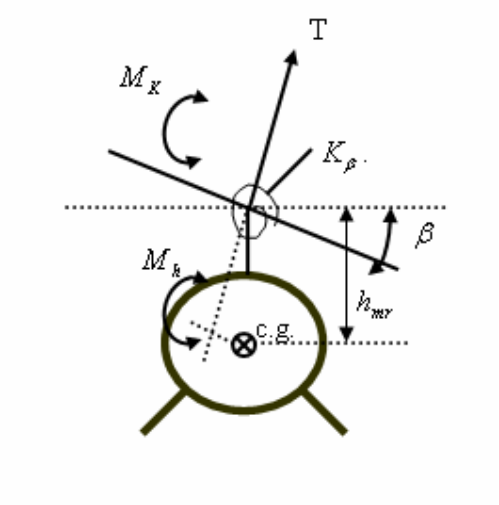

Figure 2-8 Rotor moments [4]

The moments acting on the fuselage are shown in Figure 2-8. The restraint attached to the rotor head approximated as a spring with a constant stiffness coefficient K_β. The roll moment due to restraint is $M_K = K_\beta b_1$. Assuming the thrust vector is perpendicular to the TPP, a lateral moment can be written as $M_h = Tb_1 h_{mr}$. This is due to the moment arm h_{mr} between rotor head and the center of gravity. So the total rolling moment can be written as:

$$M = (K_\beta + Th_{mr})b_1 \tag{2-45}$$

pitching moment is

$$L = (K_\beta + Th_{mr})a_1 \tag{2-46}$$

2.4.3 Fuselage Forces & Moments

The fuselage is modelled as virtual flat plate creating no lift, but drag. The drag is related to the velocity of the helicopter as shown in Eq. (2-47).

$$X_{fus} = -0.5\rho S_x u^2$$
$$Y_{fus} = -0.5\rho S_y v^2 \quad (2\text{-}47)$$
$$Z_{fus} = -0.5\rho S_z (w - V_{imr})^2$$

where S_x, S_y, S_z are the effective frontal, side and vertical drag areas of the fuselage and the u, v, w are the fuselage center of pressure velocities w.r.t to the air. The moments genetarated by fuselage drag forces is negligible under the assumption that the fuselage center of pressure coincides with the helicopter center of pressure. In order to take account of the rotor downwash on fuselage V_{imr} is added to the down velocity of the fuselage w [4].

2.4.4 Horizontal and Vertical Stabilizer Force & Moment Equations

The horizontal stabilizer produces lift and stabilizing pitching moment. The effective vertical speed at the horizontal tail location is determined by

$$w_{tr} = w - w_{wind} + l_{ht} q - K_\lambda V_{imr} \quad (2\text{-}48)$$

where the l_{ht} is the distance between the center of gravity of the helicopter and the stabilizer location (behind the cg of helicoter). K_λ (wake intensity factor) is the coefficient that represents the effect of the main rotor downwash on the stabilizer bar and the tail motor. The force produced by the stabilizer is

$$Z_{ht} = 0.5 S_{ht} (C^{ht}_{L_\infty} \mid \mu_a \mid w_{tr} + \mid w_{tr} \mid w_{tr}) \quad (2\text{-}49)$$

where the S_{ht} is the horizontal stabilizer area, $C^{ht}_{L_\infty}$ is the lift curve slope and the pitching moment is

$$M_{ht} = Z_{ht} l_{ht} \quad (2\text{-}50)$$

and the force that the vertical stabilizer produce can be calculated as in Eq. (2-51)

$$Y_{vf} = -0.5\rho S_{vf}(C_{L_\infty}^{vf} V_\infty^{tr} + |v_a|)v_a \tag{2-51}$$

where S_{vf} is the vertical fin area , $C_{L_\infty}^{vf}$ is the vertical fin lift curve slope, V_∞^{tr} is the axial velocity at the location of the tail rotor hub, u_a, v_a are the forward and side velocities w.r.t to air at the location of the vertical fin.

$$\begin{aligned} V_\infty^{tr} &= \sqrt{u_a^2 + w_{tr}^2} \\ u_a &= u - u_{wind} \\ v_a &= v - v_{wind} - \varepsilon_{vf}^{tr} V_{itr} - l_{tr} r \end{aligned} \tag{2-52}$$

Since the vertical stabilizer is near the tail rotor, it is affected by the inflow of the tail rotor. This is mentioned in the Eq. (2-52) when constructing the side velocity of the vertical stabilizer w.r.t to the air. The tail rotor flow is effective as the coefficient ε_{vf}^{tr}. The ε_{vf}^{tr} coefficient represents the fraction of the area of the vertical fin exposed to the induced velocity of the tail rotor. Vertical fin is also effected by the main rotor induced velocity and accounted as same as the horizontal stabilizer accounted. The moments that are produced because of the vertical stabilizer is positioned by offsets from the c.g. of the helicopter. Moments are

$$\begin{aligned} N_{vf} &= -Y_{vf} l_{tr} \\ L_{vf} &= -Y_{vf} h_{tr} \end{aligned} \tag{2-53}$$

2.4.5 Tail rotor Force & Moment Calculations

The tail rotor force and moment calculations are like the main rotor force and moment calculations. Since the dimension of the tail rotor is small w.r.t to the main rotor, the dynamics are much faster. Moreover, the main rotor affects the tail rotor thrust in a complex way. A complex analysis can be found in [1].

2.5 Conclusions

In this chapter, the nonlinear model of the small size helicopter with the 6DOF equations is presented. The nonlinear model is constructed based on system identification with the flight data. The nonlinear model is taken from [4]. The 6DOF equations are derived by using the Newton's second law. A linear controller can be designed by linearizing nonlinear model. In addition, 6DOF simulations can be performed.

CHAPTER 3

REALISTIC TRACK GENERATION

In realistic track generation, a priori known flight path is desired to be tracked by the helicopter. In this study, first issue is the generation of the desired path. The trajectory generation program generates the desired flight path. After the generation of the trajectory, optimization algorithm calculates the control inputs in order to minimize the error between the desired trajectory and the actual trajectory. In this study, the helicopter controlled without a conventional autopilot but with an off-line controller using optimization. The sequence of the process is given in Figure 3-1.

Figure 3-1 Trajectory generation and optimization process

3.1 Trajectory Generation

The Euler angles, angular velocities, the translational velocities and the positions define a trajectory. The apriori trajectory is found by calculating these variables. Since there are a variety of maneuvers that a helicopter can do, these maneuvers are defined in the program.

3.1.1 Maneuver

There are five distinct maneuvers defined in the trajectory generation program. These are the vertical turning, horizontal turning, hover, ascend/descend and straight flight. To create a sufficiently "rich" trajectory, a variety of these maneuvers should be used. In order to combine these maneuvers in an appropriate form the physics of these maneuvers should be known. These maneuvers are explained below.

3.1.1.1 Vertical Flight

The vertical turning maneuver is used to change the altitude of the helicopter. The turning is defined as the maximum centrifugal acceleration and the turning angle [22].

$$\frac{d\theta}{dt} = \frac{a_{centrifugal}}{V_{total}} \tag{3-1}$$

where θ is the turning angle, $a_{centrifugal}$ is the centrifugal acceleration and V_{total} is the total angle. The maneuver is shown in the Figure 3-2.

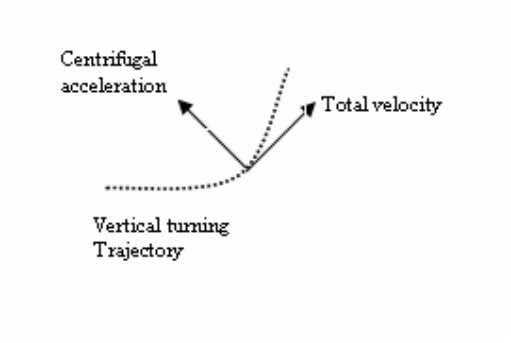

Figure 3-2 Vertical turning maneuver

In the trajectory program, the user should specify the maximum centrifugal acceleration and the turning angle.

3.1.1.2 Horizontal Flight

The horizontal turning maneuver is used to change the heading of the helicopter. The horizontal flight is defined as same as the vertical flight. The trajectory generation program generates the horizontal flight by using the bank-to-turn maneuver. The max roll rate of the helicopter is required in order to calculate the maneuver. The bank-to-turn maneuver is simply turning the heading of the helicopter by rolling. This is shown in the Figure 3-3.

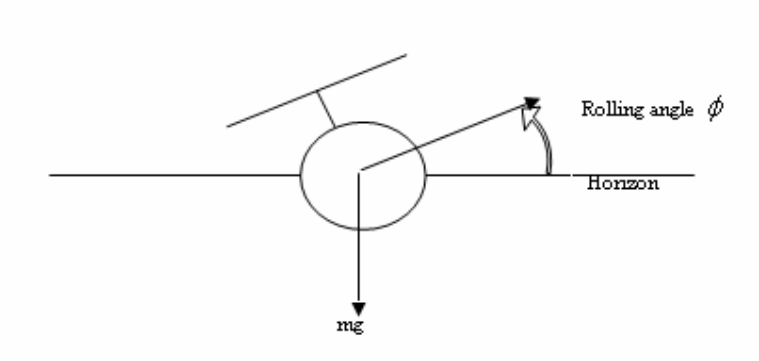

Figure 3-3 .Horizontal turning maneuver

3.1.1.3 Hover

Hover is a special maneuver for helicopters. By this maneuver, the helicopter can keep its position constant. The trajectory generation program decelerates the helicopter if it has initial velocity before the maneuver starts.

3.1.1.4 Ascend/Descend

Ascending or descending maneuvers are similar maneuvers with minor differences. The former one rises the helicopter up while the latter one takes the helicopter down. This maneuver is different from the vertical turning. The helicopter does not have forward velocity when it ascends/descends.

3.1.1.5 Straight Flight

Straight flight takes the helicopter forward. By this maneuver, a helicopter can be accelerated or decelerated towards the nose of the helicopter. This maneuver can be generated independently. In addition, this maneuver should be used just before and after a vertical flight and a horizontal flight. An example of a trajectory is given in Figure 3-4.

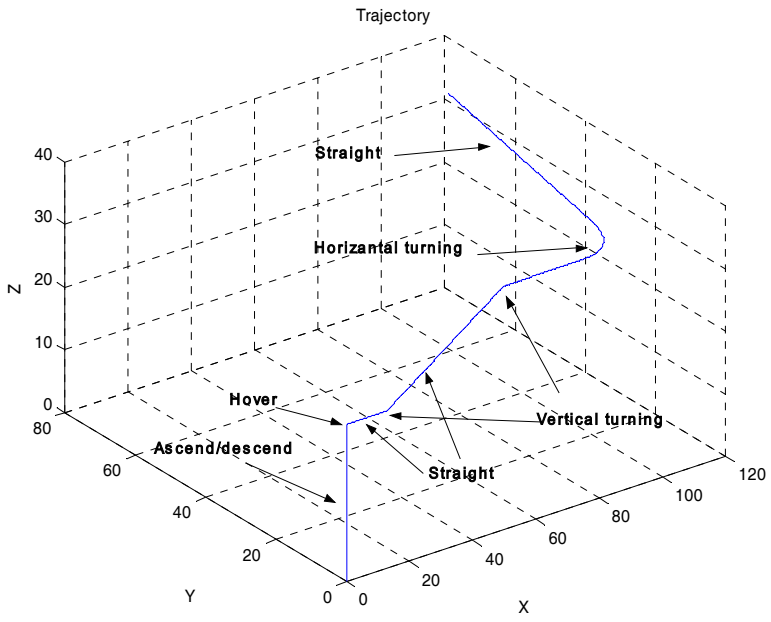

Figure 3-4 Trajectory example

3.2 Optimization Algorithm

In the optimization algorithm, the steepest descent method is used in order to minimize the cost function.

The optimization problem is defined as of finding the control inputs for the helicopter model in order to take the helicopter to the desired positions that are found before the flight. The helicopter should follow the desired positions and the velocities in order to track the desired trajectory. Since the rotational motion affects the motion in Earth-fixed reference frame, helicopter should track the Euler angles too. However, the helicopter cannot track the Euler angles exactly because of the trim conditions of the helicopter. Instead of tracking the Euler angles, the helicopter tracks the desired angular velocities. The cost function is similar to the one shown in Eq. (3-2)

$$J(\theta_{control}) = \alpha_1 \int_0^t (\overline{V}_{des} - \overline{V}_{act})dt + \alpha_2 \int_0^t (\overline{W}_{des} - \overline{W}_{act})dt + \alpha_3 \int_0^t (\overline{P}_{des} - \overline{P}_{act})dt \quad (3\text{-}2)$$

where V is velocity of the helicopter W is angular velocity and P is the position of the helicopter.

The helicopter has four control inputs and these control inputs have limitations. In order to account these limitations and to have an unconstrained optimization, the constraints are embedded in the cost function as penalty functions. The constraints are like below

$$C_1 = \kappa(\max(\theta_{\max}, \theta_{actual}) - \theta_{\max}) \quad (3\text{-}3)$$

$$C_2 = \kappa abs(\min(\theta_{\min}, \theta_{actual}) - \theta_{\min}) \quad (3\text{-}4)$$

where κ is large positive scalar. The new cost function becomes like in Eq. (3-5).

$$J_d = J(\theta_{control}) + \sum_{i=1}^{8} C_i \quad (3\text{-}5)$$

Since there are four control inputs, there are eight constraints. This cost function is minimized subject to the helicopter model and the equations of motion. Another constraint is the total velocity of the helicopter. The helicopter model is valid up to

the 20m/sec ($\mu < 0.15$) total velocity. This constraint is added to the cost function as well.

$$J_d = J(\theta_{control}) + \sum_{i=1}^{8} C_i + \kappa * \max((V_{total}, 20) - 20) \tag{3-6}$$

To have the steepest descent algorithm working, the gradient vector of the control inputs should be found. The gradient of the control inputs w.r.t the cost function is found by numerical differentiation.

$$\frac{\partial J}{\partial \theta_{mainrotor}} = \frac{J(\theta_{mainrotor} + \varepsilon) - J(\theta_{mainrotor})}{\varepsilon} \tag{3-7}$$

$$\frac{\partial J}{\partial \theta_{tailrotor}} = \frac{J(\theta_{tailrotor} + \varepsilon) - J(\theta_{tailrotor})}{\varepsilon} \tag{3-8}$$

$$\frac{\partial J}{\partial \theta_{longitudinal}} = \frac{J(\theta_{longitudinal} + \varepsilon) - J(\theta_{longitudinal})}{\varepsilon} \tag{3-9}$$

$$\frac{\partial J}{\partial \theta_{lateral}} = \frac{J(\theta_{lateral} + \varepsilon) - J(\theta_{lateral})}{\varepsilon} \tag{3-10}$$

After getting the gradient vector, one-dimensional search runs to have the minimum cost function. In one-dimensional search, a positive scalar α is searched. The α scalar is chosen to minimize the cost function along the negative gradient vector direction of the control inputs.

$$J(\theta_k) > J(\theta_k - \alpha * \nabla J) \tag{3-11}$$

$$\begin{aligned} &J(\theta_k - \alpha * \nabla J) < J(\theta_k - \beta \nabla J) \\ &\alpha < \beta \end{aligned} \tag{3-12}$$

In Eq. (3-12), a new scalar β is to be found so that one has a graph like Figure 3-5.

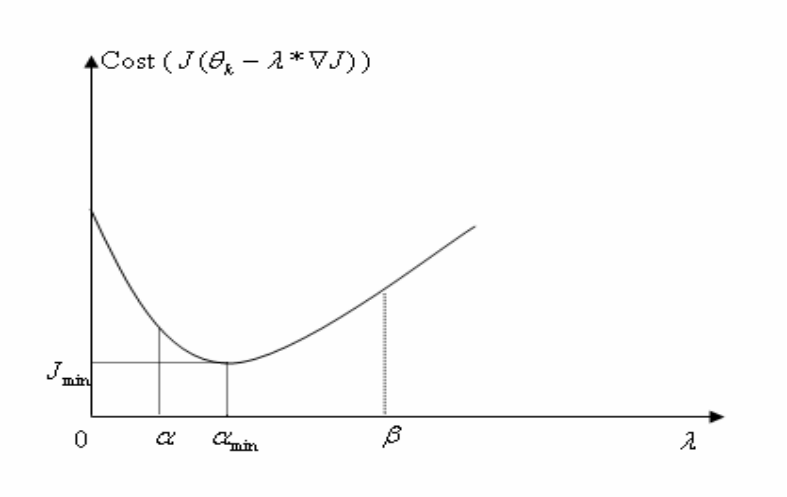

Figure 3-5 One dimensional search

The interval between α and β is divided into equal parts and the cost function is evaluated at each segment. The scalar λ that minimizes the cost function is found by sorting the cost values evaluated at each λ.

The optimization is done at blocks of the time of the flight. The blocks are named as optimization steps. When the optimization of one block finishes the outputs of this time block is transferred to the next time block. The new optimization starts with the initial values that are the last values of the last block. The optimization timeline is shown in the Figure 3-6.

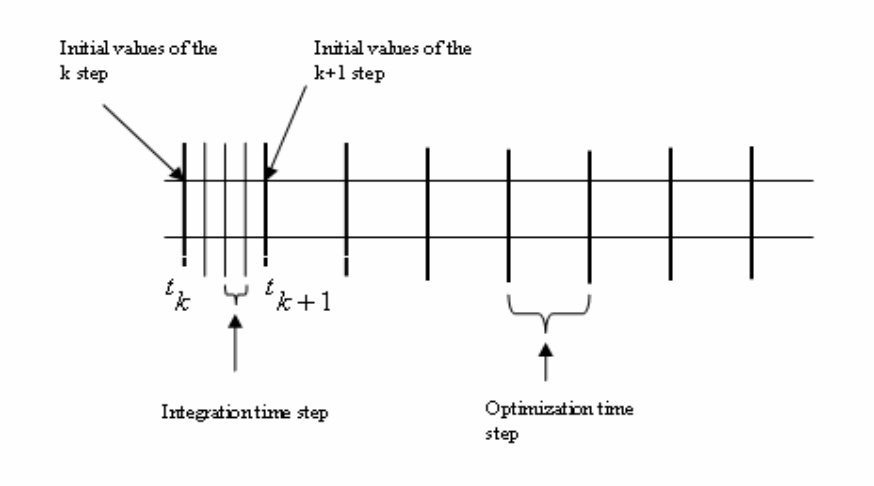

Figure 3-6 The optimization time step

3.3 Results

The trajectory shown in Figure 3-8 is the output of the trajectory generation program. The optimization program takes the output of the trajectory generation program in order to find the control inputs. Then the helicopter model is driven by the control inputs found by the optimization program. The states are shown in Figure 3-7 and the trajectory is shown in Figure 3-8. From the Figure 3-7, the actual and the desired values of body rates p , q and Euler angles ϕ and θ are not fit well. The reason for the difference is that the trajectory generation algorithm takes account only the kinematic relations not the dynamic relations. However, the helicopter can only have a forward velocity with accompanying pitch angle θ . In addition; the helicopter sustains its side velocity as zero with some non-zero bank angle ϕ since the tail rotor generates side velocity while counteracting the main rotor torque. The other actual states are fit well with the desired states by decreasing the importance of the body rates p , q and Euler angles ϕ and θ in the cost function.

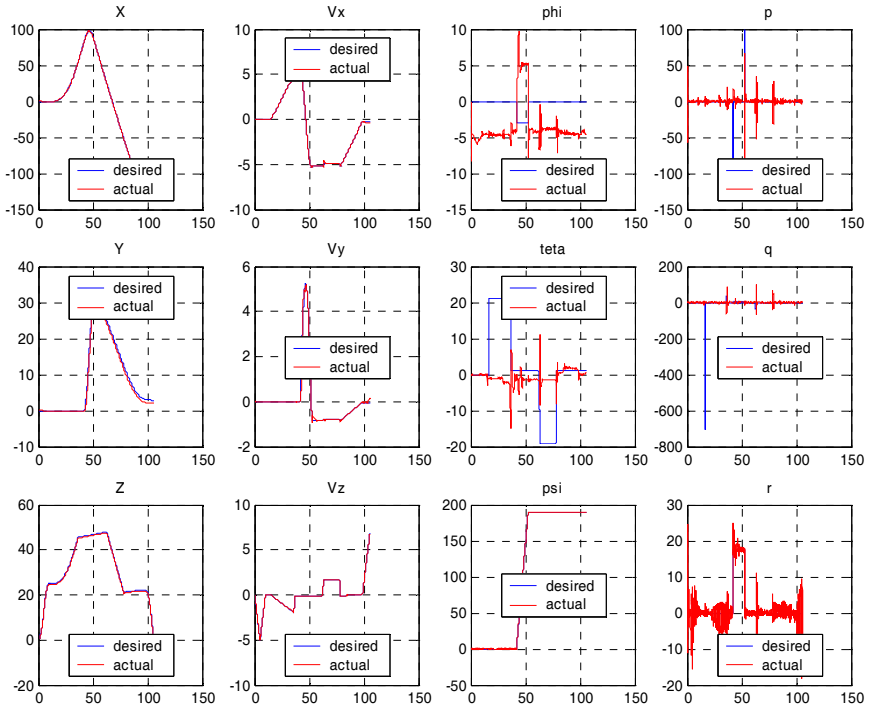

Figure 3-7 States of the system

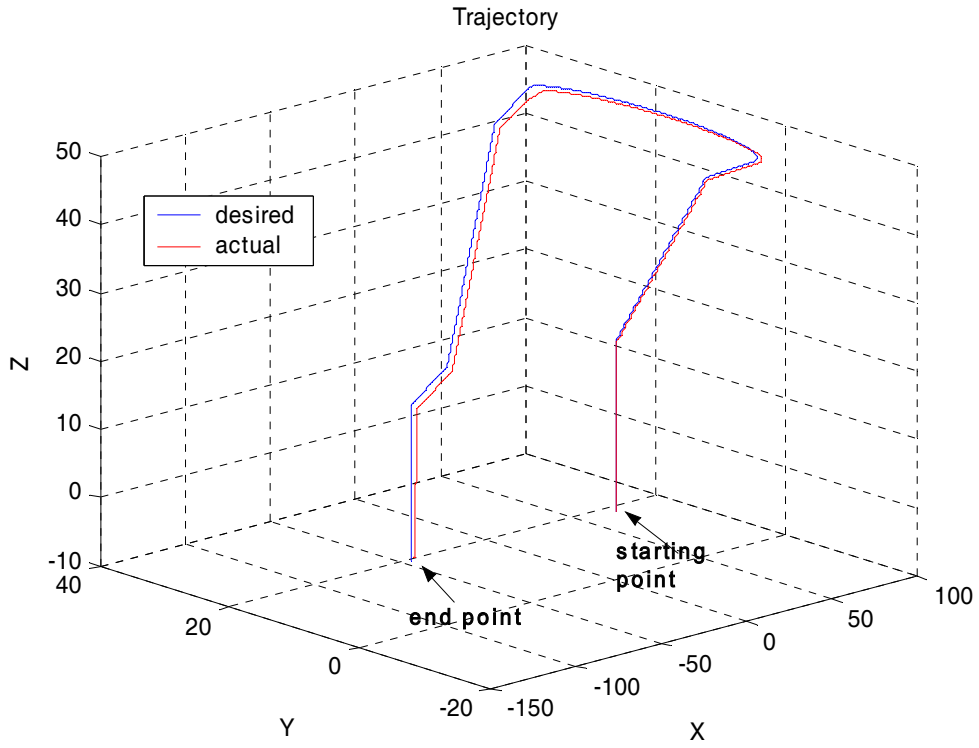

Figure 3-8 Actual and desired trajectories

CHAPTER 4

TRIMMING & LINEARIZATION

In this chapter, trimming and linearization methods are introduced. The linear control techniques are used to design the controllers for aerial vehicles. Designing linear control laws for nonlinear systems are accomplished by linearization of the nonlinear system. Taylor's series expansion of the nonlinear system is used for linearization. The linear controller design is based on the small perturbation theory. Mainly the theory says that the motion of the helicopter is described as the disturbed motion from the trim point. The validity of the linearization depends on the behavior of the forces at small amplitudes so that the dominant effect should be linear [1]. In order to control the system, the linearization should be done around the trim point. By this way, the linear system will reflect the character of the nonlinear system.

The tendency of the helicopter to return to the trim point or to depart from it can be determined by the linearized model coefficients at the trim points of a nonlinear model. This tendency is called as *static stability*. The coefficients of the model of the aircraft in linearization are called as *stability derivatives*. These coefficients can be determined by analytical or numerical differentiation. In this thesis, both methods are implemented. The performances of these methods are tested by the nonlinear model at the trim point. Small control deviations from the trim points are introduced to each of the linear models and the nonlinear model. The trajectories of the states are observed in a time interval.

4.1 Trimming

The physical meaning of trim point is the equilibrium point of helicopter equations of motion that and it can be done by nulling of the derivatives in the body coordinate system.

Nulling the derivatives of the motion means inserting zeros to the left hand-side of the Eq. (4-1)

$$\begin{aligned}
\dot{U} &= V_e R_e - W_e Q_e - g\sin\theta_e + (X_{mr} + X_{fus})/m \\
\dot{V} &= W_e P_e - U_e R_e + g\sin(\Phi_e)\cos(\theta_e) + (Y_{mr} + Y_{fus} + Y_{tr} + Y_{vf})/m \\
\dot{W} &= U_e Q_e - V_e P_e + g\cos(\Phi_e)\cos(\theta_e) + (Z_{mr} + Z_{fus} + Z_{ht})/m \\
\dot{P} &= Q_e R_e (I_{zz} - I_{yy})/I_{xx} + (L_{mr} + L_{vf} + L_{tr})/I_{xx} \\
\dot{Q} &= P_e R_e (I_{xx} - I_{zz})/I_{yy} + (M_{mr} + M_{ht})/I_{yy} \\
\dot{R} &= P_e Q_e (I_{yy} - I_{xx})/I_{zz} + (-Q_e + N_{vf} + N_{tr})/I_{zz}
\end{aligned} \tag{4-1}$$

where the force and moments produced by the helicopter components are written as the summation. *mr* represents for the main rotor, *fus* for fuselage, *tr* for tail rotor, *vf* for vertical fin and *ht* for the horizontal stabilizer.

The Euler angles are given by the relationship between the body axis angular rates and the rate of change of euler angle $\dot{\Psi}$, the turn rate about the vertical axis in Eq. (4-2).

$$\begin{aligned}
P_e &= -\dot{\Psi}_e \sin(\theta_e) \\
Q_e &= \dot{\Psi}_e \sin(\Phi_e)\cos(\theta_e) \\
R_e &= \dot{\Psi}_e \cos(\Phi_e)\cos(\theta_e)
\end{aligned} \tag{4-2}$$

The combination of Eq. (4-1) and Eq. (4-2) results 9 equations with 13 unknowns. To define a unique solution, four variables must be prescribed. The prescribed variables are chosen as forward velocity u_e, side velocity v_e, vertical velocity w_e, and turn rate $\dot{\Psi}$. Other than these prescribed variables, there are unknown flight states need to be estimated before the trim algorithm runs. The trim solution is

found by an iterative algorithm to obtain the converged values of the estimated variables. The summary of the method is given in Figure 4-1. The estimated flight states are the pitch and roll Euler angles θ_e and ϕ_e, the main rotor and the tail rotor downwash λ_0 and λ_{0T}, the longitudinal flap angle and lateral flap angle a_1 and b_1.

Figure 4-1 Trim process

The first stage of the trim process is to calculate the thrust of the main rotor by using Eq. (4-3). The Eq. (4-3) is derived from the Eq. (4-1). The fuselage and horizontal force Z_{fus} and Z_{ht} are functions of translational velocities and translational velocities are known since they are the prescribed variables. The right hand side of Eq. (4-3) is calculated by using the estimated Euler pitch and roll angles. The body rates p and q are found by using the prescribed variable $\dot{\psi}$ in Eq. (4-2). The thrust Z_{mr} is found by rewriting the Eq. (4-3).

$$Z_{fus} + Z_{mr} + Z_{ht} = [vp - uq - g\cos(\theta)\cos(\Phi)]m \tag{4-3}$$

The main rotor inflow can be found by the relations in Eq. (4-4) and Eq. (4-5). The thrust coefficient calculated by using Eq.(4-4) is used in Eq. (4-5) in order to find the inflow.

$$T_{mr} = C_T\left(\rho(\Omega R)^2 \pi R^2\right) \tag{4-4}$$

$$\lambda_0 = \frac{C_T}{2n_w\sqrt{\left(\mu^2 + (\lambda_0 - \mu_z)^2\right)}} \tag{4-5}$$

The λ_0 is an estimated variable. At this point, a comparison with the estimated value of the inflow and the calculated value of the inflow is made; If the difference between two values is in the tolerance region then the inflow and the thrust coefficient are found. Otherwise, the iterative scheme used for finding the main rotor inflow given in Eq. (4-6) is utilized. The condition given in Eq. (4-7) is tested at the end of each iteration to stop the algorithm.

$$\begin{aligned}
&\lambda_{0,i+1} = \lambda_{0,i} + k_{\lambda 0} h_i(\lambda_{0,i}) \\
&h_i = -\frac{(2\lambda_{0,i}\Lambda^{1/2} - C_T)\Lambda}{2\Lambda^{3/2} + a_0 s\Lambda/4 - C_T(\mu_z - \lambda_{0,i})} \\
&\Lambda = \mu^2 + (\lambda_{0,i} - \mu_z)^2 \\
&|\lambda_{0,i+1} - \lambda_{0,i}| < v_{\lambda 0}\,|\lambda_{0,i}|
\end{aligned} \tag{4-6}$$

$$| \lambda_{0,k+1} - \lambda_{0,k} | < v_{\lambda k} | \lambda_{0,k} | \tag{4-7}$$

The tail thrust and the tail inflow can be calculated by using the same scheme used in calculation of the main rotor thrust. In Eq. (4-8), the main rotor torque, the tail rotor thrust and the vertical stabilizer equations are taken into consideration and it is taken from Eq.(4-1). The main rotor torque calculations are straightforward after the main rotor calculations have been converged. The vertical stabilizer force is a function of translational velocities and the angular rates.

$$-Q_e + N_{vf} + N_{tr} = P_e Q_e (I_{yy} - I_{xx}) \tag{4-8}$$

At this point, all the external forces and moments can be found since they are functions of main rotor force T and tail rotor force T_t and translational velocities (u, v, w) and angular velocities (p, q, r) and Euler angles (θ, ϕ). The estimated variables (θ, ϕ, a_1, b_1) are calculated by using Eq. (4-1) in order to compare the estimated values and the calculated values. The trim process is finished if the difference between the estimated variables and the calculated variables are in the tolerance region.

4.2 Linearization

Consider the helicopter equations of motion described in nonlinear form as.

$$\dot{\mathbf{x}} = \mathbf{F}(\mathbf{x}, \mathbf{u}, t) \tag{4-9}$$

The linearized equations of motion for the six degrees of freedom can be written as

$$\dot{\mathbf{x}} = \mathbf{A}\mathbf{x} + \mathbf{B}\mathbf{u} \tag{4-10}$$

where $\mathbf{x} = \begin{pmatrix} u & w & q & \theta & a_1 & v & p & \phi & r & b_1 \end{pmatrix}$ is the state column and $\mathbf{u} = \begin{pmatrix} \theta_0 & \theta_{1s} & \theta_{1c} & \theta_{0T} \end{pmatrix}$ are the control inputs, where

$$\mathbf{A} = \left(\frac{\partial \mathbf{F}}{\partial \mathbf{x}} \right)_{\mathbf{X}=\mathbf{X}_e} \tag{4-11}$$

$$\mathbf{B} = \left(\frac{\partial \mathbf{F}}{\partial \mathbf{u}} \right)_{\mathbf{X}=\mathbf{X}_e} \tag{4-12}$$

The heading angle Ψ is omitted because the direction of the flight in the horizontal plane does not affect the aerodynamic or dynamic forces and moments.

$$\mathbf{A} = \begin{bmatrix}
X_u & X_w - q_e & X_q - w_e & -g\cos(\theta_e) & X_{a_1} & X_v + r_e & X_p & 0 & X_r + v_e & 0 \\
Z_u + q_e & Z_w & Z_q + u_e & -g\cos(\phi_e)\sin(\theta_e) & Z_{a_1} & Z_v - p_e & Z_p - v_e & -g\cos(\phi_e)\cos(\theta_e) & Z_r & 0 \\
M_u & M_w & M_q & 0 & M_{a_1} & M_v & M_p & 0 & M_r & 0 \\
0 & 0 & \cos(\phi_e) & 0 & 0 & 0 & 0 & 0 & \sin(\phi_e) & 0 \\
0 & 0 & -1 & 0 & -1/\tau & 0 & 0 & 0 & 0 & 0 \\
Y_u - r_e & Y_w + p_e & Y_{q''} & Y_\theta - g\sin(\phi_e)\sin(\theta_e) & Y_{a_1} & Y_v & Y_p + w_e & Y_\phi + g\cos(\phi_e)\cos(\theta_e) & Y_r - u_e & Y_{b_1} \\
L_u & L_w & L_q & L_\theta & L_{a_1} & L_v & L_p & L_\phi & L_r & L_{b_1} \\
0 & 0 & \sin(\phi_e)\tan(\theta_e) & 0 & 0 & 0 & 1 & 0 & \cos(\phi_e)\tan(\theta_e) & 0 \\
N_u & N_w & N_q & N_\theta & N_{a_1} & N_v & N_p & N_\phi & N_r & N_{b_1} \\
0 & 0 & 0 & 0 & 0 & 0 & -1 & 0 & 0 & -1/\tau
\end{bmatrix} \tag{4-13}$$

where τ is the rotor time constant.

$$\mathbf{B} = \begin{bmatrix}
0 & 0 & 0 & 0 \\
Z_{\theta_0} & 0 & 0 & 0 \\
0 & 0 & 0 & 0 \\
0 & 0 & 0 & 0 \\
0 & A_{\delta_{lon}} & 0 & 0 \\
0 & 0 & 0 & 0 \\
0 & 0 & 0 & 0 \\
0 & 0 & 0 & 0 \\
0 & 0 & 0 & N_{\theta_T} \\
0 & 0 & B_{\delta_{lat}} & 0
\end{bmatrix} \tag{4-14}$$

4.2.1 Analytic Linearization

Analytic linearization is based on the nonlinear model introduced in chapter II. The dominant derivatives [5] are derived in this section. The external forces and moments are assumed to be linear functions of the states for small perturbations. The derivatives given in this section are found by using analytic relations between the external forces, moments and the states.

4.2.1.1 Velocity derivatives $\mathbf{X_u}$ and $\mathbf{Y_v}$

Velocity perturbations give rise to rotor flapping, changes in rotor lift and drag and the incidence and sideslip angles of the flow around the fuselage and empennage. In high speed flight X_u and Y_v are practically linear with speed and reflect the drag and side force on the rotor-fuselage combination respectively. The derivatives are principally due to the disc tilts to aft and port following perturbations in u and v.

From Eq. (4-1) we have

$$\begin{aligned} \dot{u} &= vr - wq - g\sin(\theta) + (X_{mr} + X_{fus})/m \\ f_1 &= (X_{mr} + X_{fus})/m \\ X_u &= \frac{\partial f_1}{\partial u} \\ \frac{\partial f_1}{\partial u} &= \frac{1}{m}\frac{\partial (X_{mr} + X_{fus})}{\partial u} \end{aligned} \qquad (4\text{-}15)$$

To find X_u the force components due to the helicopter are differentiated w.r.t u as in Eq. (4-16) and Eq. (4-17). In Eq. (4-16), the force produced by the main rotor is considered and in Eq. (4-17), the force produced by the fuselage is considered.

$$
\begin{aligned}
&\frac{\partial X_{mr}}{\partial u}=\frac{\partial (Ta_1)}{\partial u}=\frac{\partial T}{\partial u}a_1+T\frac{\partial a_1}{\partial u}\\
&\frac{\partial T}{\partial u}=\rho(\Omega R)^2\pi R^2\frac{\partial C_T}{\partial u}\\
&\frac{\partial C_T}{\partial u}=\frac{a\sigma}{2}(\theta_0(\partial\mu/\partial u)+\frac{-1}{2}\frac{\partial\lambda_0}{\partial u})\\
&\frac{\partial\mu}{\partial u}=\frac{u}{(\sqrt{u^2+v^2})\Omega R}\\
&\frac{\partial\lambda_0}{\partial u}=\frac{\frac{C_T a\sigma\theta_0 u}{(\Omega R)^2}-\frac{8\eta_w^2\lambda_0^2 u}{(\Omega R)^2}}{8\lambda_0\eta_w^2(\mu^2+(\lambda_0-\mu_z)^2)+8\eta_w^2\lambda_0^2(\lambda_0-\eta_z)+C_T a\sigma/2}\\
&\frac{\partial a_1}{\partial u}=\frac{\partial a_1}{\partial\mu}\frac{\partial\mu}{\partial u}=2K_\mu(\frac{4\theta_0}{3}-\lambda_0)(\frac{u}{(\sqrt{u^2+v^2})\Omega R})
\end{aligned}
\tag{4-16}
$$

$$
\begin{aligned}
&\frac{\partial X_{fus}}{\partial u}=\begin{cases}0.5\rho S_x^{fus}u\frac{\partial V_{imr}}{\partial u}+0.5\rho S_x^{fus}V_{imr} & u<V_{imr}\\ -0.5\rho S_x^{fus}u\frac{\partial V_\infty}{\partial u}-0.5\rho S_x^{fus}V_\infty & u>V_{imr}\end{cases}\\
&\frac{\partial V_\infty}{\partial u}=\frac{(u+2(w+V_{imr})\frac{\partial V_{imr}}{\partial u}}{\sqrt{u^2+v^2+(w+V_{imr})^2}}\\
&\frac{\partial V_{imr}}{\partial u}=\Omega R\frac{\partial\lambda_0}{\partial u}
\end{aligned}
\tag{4-17}
$$

The same procedure is used to derive the Y_v in Eq. (4-18).

$$
\begin{aligned}
&\dot{v}=wp-ur+g\sin(\Phi)\cos(\Theta)+(Y_{mr}+Y_{fus}+Y_{tr}+Y_{vf})/m\\
&f_2=(Y_{mr}+Y_{fus}+Y_{tr}+Y_{vf})/m\\
&Y_v=\frac{\partial f_2}{\partial v}\\
&\frac{\partial f_2}{\partial v}=\frac{1}{m}\frac{\partial(Y_{mr}+Y_{fus}+Y_{tr}+Y_{vf})/m}{\partial v}
\end{aligned}
\tag{4-18}
$$

The differentiation is done w.r.t v by considering the forces produced by the main rotor, fuselage, tail rotor and vertical stabilizer in Eqns. (4-19), (4-20), (4-21), and Eq. (4-22), respectively.

$$\frac{\partial Y_{mr}}{\partial v} = \frac{\partial (Tb_1)}{\partial v} = \frac{\partial T}{\partial v} b_1 + T \frac{\partial b_1}{\partial v}$$
$$\frac{\partial T}{\partial v} = \rho (\Omega R)^2 \pi R^2 \frac{\partial C_T}{\partial v}$$
$$\frac{\partial C_T}{\partial v} = \frac{a\sigma}{2} (\theta_0 (\partial \mu / \partial v) + \frac{-1}{2} \frac{\partial \lambda_0}{\partial v})$$
$$\frac{\partial \mu}{\partial v} = \frac{v}{(\sqrt{u^2 + v^2}) \Omega R} \qquad (4\text{-}19)$$
$$\frac{\partial \lambda_0}{\partial v} = \frac{\frac{C_T a \sigma \theta_0 v}{(\Omega R)^2} - \frac{8 \eta_w^2 \lambda_0^2 v}{(\Omega R)^2}}{8 \lambda_0 \eta_w^2 (\mu^2 + (\lambda_0 - \mu_z)^2) + 8 \eta_w^2 \lambda_0^2 (\lambda_0 - \eta_z) + C_T a \sigma / 2}$$
$$\frac{\partial b_1}{\partial v} = \frac{\partial b_1}{\partial \mu} \frac{\partial \mu}{\partial v} = -2 K_\mu (\frac{4\theta_0}{3} - \lambda_0)(\frac{v}{(\sqrt{u^2 + v^2}) \Omega R})$$

$$\frac{\partial Y_{fus}}{\partial v} = \begin{cases} 0.5 \rho S_y^{fus} v \frac{\partial V_{imr}}{\partial v} + 0.5 \rho S_{yx}^{fus} V_{imr} & u < V_{imr} \\ -0.5 \rho S_y^{fus} v \frac{\partial V_\infty}{\partial v} - 0.5 \rho S_y^{fus} V_\infty & u > V_{imr} \end{cases}$$
$$\frac{\partial V_\infty}{\partial v} = \frac{(v + 2(w + V_{imr}) \frac{\partial V_{imr}}{\partial v}}{\sqrt{u^2 + v^2 + (w + V_{imr})^2}} \qquad (4\text{-}20)$$
$$\frac{\partial V_{imr}}{\partial v} = \Omega R \frac{\partial \lambda_0}{\partial v}$$

$$
\begin{aligned}
&\frac{\partial Y_{tr}}{\partial v} = \rho(\Omega_{tr} R_{tr})\pi R_{tr}^2 \frac{\partial C_{Tt}}{\partial v} \\
&\frac{\partial C_{Tt}}{\partial v} = \frac{a_{tr}\sigma_{tr}}{4}\left(\frac{\partial \mu_{ZT}}{\partial v} - \frac{\partial \lambda_{0T}}{\partial v}\right) \\
&\frac{\partial \lambda_{0T}}{\partial v} = \frac{\dfrac{C_{Tt} a_t \sigma_t / 2}{\Omega_{tr} R_{tr}} - \dfrac{8\lambda_{0T}^2(\mu_{ZT} - \lambda_{0T})}{\Omega_{tr} R_{tr}}}{8\lambda_{0T}(\mu_T^2 + (\mu_{ZT} - \lambda_{0T})^2) - 8\lambda_{0T}^2(\mu_{ZT} - \lambda_{0T}) + C_{Tt} a_t \sigma_t / 2} \\
&\frac{\partial \mu_{ZT}}{\partial v} = \frac{1}{\Omega_{tr} R_{tr}}
\end{aligned}
\qquad (4\text{-}21)
$$

$$
\begin{aligned}
&\frac{\partial Y_{vf}}{\partial v} = -0.5\rho S_{vf}\left(C_{L\alpha}^{vf} V_{\infty}^{tr} + |v_{vf}|\right)\frac{\partial v_{vf}}{\partial v} - 0.5\rho S_{vf}\left(C_{L\alpha}^{vf}\left(-\frac{w_{tr}\dfrac{\partial w_{tr}}{\partial v}}{\sqrt{u^2 + w_{tr}^2}}\right) + sign(v_{vf})\frac{\partial v_{vf}}{\partial v}\right)v_{vf}\Big) \\
&\frac{\partial v_{vf}}{\partial v} = 1 - \varepsilon_{tr}^{vf}\frac{\partial V_{itr}}{\partial v} \\
&\frac{\partial V_{itr}}{\partial v} = \Omega_{tr} R_{tr}\frac{\partial \lambda_{0T}}{\partial v} \\
&\frac{\partial w_{tr}}{\partial v} = -K_{\lambda}\frac{\partial V_{imr}}{\partial v} \\
&\frac{\partial V_{imr}}{\partial v} = \Omega R\frac{\partial \lambda_0}{\partial v}
\end{aligned}
\qquad (4\text{-}22)
$$

4.2.1.2 The Speed and Incidence Derivatives $\mathbf{M_u}$, $\mathbf{M_w}$

Speed and incidence static stability derivatives, have major effect on longitudinal stability. The aerodynamic load on the fuselage is a function of the forward velocity. Mainly the pitching moment is produced at the centre of the mass by the horizontal stabilizer with increasing forward velocity due to the aerodynamic load on the horizontal stabilizer. In addition the main rotor disc flaps back with increasing forward velocity resulting a nose up pitching moment and a tendency to reduce the speed [1]. M_u is derived by differentiation of moments produced by the main rotor and the horizontal stabilizer w.r.t u as

$$\frac{\partial M}{\partial u} = \frac{\partial \left(M_{mr} + M_{ht} \right)}{\partial u}$$

$$\frac{\partial M_{mr}}{\partial u} = \frac{\partial \left(K_{\beta} + Th_{mr} \right) a_1}{\partial u} = \frac{\partial T}{\partial u} a_1 + \left(K_{\beta} + Th_{mr} \right) \frac{\partial a_1}{\partial u} \tag{4-23}$$

$$\frac{\partial M_{ht}}{\partial u} = \frac{\partial M_{ht}}{\partial u} 0.5 \rho S_{ht} (C_{L\alpha}^{ht} sign(u) w_{ht}) l_{ht} + 0.5 \rho S_{ht} (C_{L\alpha}^{ht} |u| \frac{\partial w_{ht}}{\partial u} + 2 sign(w_{ht}) w_{ht} \frac{\partial w_{ht}}{\partial u}) l_{ht}$$

$$w_{ht} = w + l_{ht} q - K_{\lambda} V_{imr}$$

The expanded forms of $\frac{\partial T}{\partial u}$ and $\frac{\partial a_1}{\partial u}$ are in Eq. (4-24).

A positive perturbation in normal velocity w will increase the lift produced by the main rotor disc. However, the advancing side of the disc will produce more lift than the retreating side while in forward flight due to the translational motion difference between the sides of the rotor disc. The increase in the unbalance of lift causes the rotor disc flaps back giving rise to pitching moment.

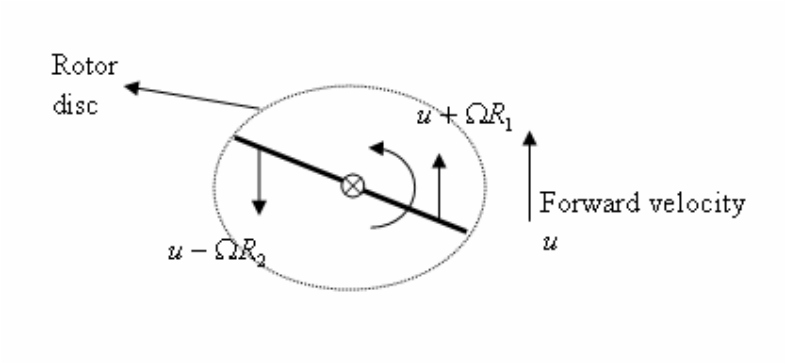

Figure 4-2 Main rotor disc in forward flight

$$\frac{\partial M}{\partial w}=\frac{\partial\left(M_{mr}+M_{ht}\right)}{\partial w}$$

$$\frac{\partial M_{mr}}{\partial w}=\frac{\partial\left(K_{\beta}+Th_{mr}\right)a_1}{\partial w}=\frac{\partial T}{\partial w}a_1+\left(K_{\beta}+Th_{mr}\right)\frac{\partial a_1}{\partial w}$$

$$\frac{\partial M_{ht}}{\partial w}=\frac{\partial\left(0.5\rho S_{ht}(C_{L\alpha}^{ht}\mid u\mid w_{ht}+\mid w_{ht}\mid w_{ht})l_{ht}\right)}{\partial w}$$

$$\frac{\partial M_{ht}}{\partial w}=\left\{\begin{array}{ll}0.5\rho S_{ht}(C_{L\alpha}^{ht}\mid u\mid+sign(w_{ht})w_{ht}+\mid w_{ht}\mid)l_{ht} & K_{\lambda}=0\\ 0.5\rho S_{ht}(C_{L\alpha}^{ht}\mid u\mid\frac{\partial w_{ht}}{\partial w}+(sign(w_{ht})w_{ht}\frac{\partial w_{ht}}{\partial w})+\mid w_{ht}\mid\frac{\partial w_{ht}}{\partial w})l_{ht} & K_{\lambda}\neq 0\end{array}\right\}$$

$$\frac{\partial w_{ht}}{\partial w}=\left\{\begin{array}{ll}1 & K_{\lambda}=0\\ -\frac{\partial V_{imr}}{\partial w}K_{\lambda}-V_{imr}\frac{\partial K_{\lambda}}{\partial w} & K_{\lambda}\neq 0\end{array}\right\}$$

$$\frac{\partial V_{imr}}{\partial w}=\Omega R\frac{\partial\lambda_0}{\partial w}$$

$$\frac{\partial K_{\lambda}}{\partial w}=\frac{-1.5u(\frac{\partial V_{imr}}{\partial w}-1)}{((V_{imr}-w)(g_f-g_i))^2} \qquad (4\text{-}24)$$

4.2.1.3 The Dihedral and Weathercock Derivatives $\mathbf{L_v}$ and $\mathbf{N_v}$

Velocity derivatives belong to the lateral-directional degrees of freedom and the most significant ones are the sideslip derivatives- the dihedral effect L_v and the weathercock stability N_v. The magnitudes of these two moments as sideslip increases determine the lateral-directional static stability characteristic. A positive value of N_v is stabilizing, while a negative value of L_v is stabilizing [1].

$$\frac{\partial L}{\partial v}=\frac{\partial(L_{mr}+L_{vf}+L_{tr})}{\partial v} \qquad (4\text{-}25)$$

The dihedral effect, L_v, mainly depends on the main rotor. As in the M_u derivative, the main rotor blades produce unbalance lift and the helicopter tends to roll.

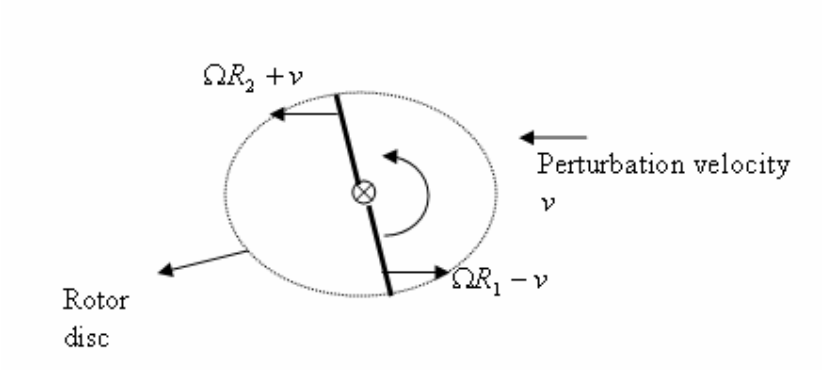

Figure 4-3 Main rotor disc perturbed by side velocity

$$\frac{\partial L_{mr}}{\partial v} = \frac{\partial\left(K_\beta + Th_{mr}\right)b_1}{\partial v} = \frac{\partial T}{\partial v} b_1 + \left(K_\beta + Th_{mr}\right)\frac{\partial b_1}{\partial v}$$

$$\frac{\partial T}{\partial v} = \frac{\partial\left(\rho(\Omega R)^2 \pi R^2 C_T\right)}{\partial v}$$

$$\frac{\partial C_T}{\partial v} = \frac{a\sigma}{2}(\theta_0(\frac{1}{3} + \partial\mu/\partial v) + \frac{-1}{2}\frac{\partial\lambda_0}{\partial v})$$

$$\frac{\partial \mu}{\partial v} = -\frac{v}{(\sqrt{u^2+v^2})\Omega R} \qquad (4\text{-}26)$$

$$\frac{\partial \lambda_0}{\partial v} = \frac{-\frac{C_T a\sigma\theta_0 v}{(\Omega R)^2} + \frac{8\eta_w^2\lambda_0^2 v}{(\Omega R)^2}}{8\lambda_0\eta_w^2(\mu^2 + (\lambda_0 - \mu_z)^2) + 8\eta_w^2\lambda_0^2(\lambda_0 - \eta_z) + C_T a\sigma/2}$$

$$\frac{\partial b_1}{\partial v} = -2K_\mu\left(\frac{4\theta_0}{3} - \lambda_0\right)(-\frac{v}{(\sqrt{u^2+v^2})\Omega R})$$

The tail rotor and the vertical fins' effects are proportional to their lever arm. Their lever arm is defined as the height of their position from the centre of mass. Their effects are shown in Eq. (4-27) and in Eq. (4-28).

$$\frac{\partial L_{tr}}{\partial v} = \frac{\partial (Y_{tr})}{\partial v} h_{tr}$$
$$\frac{\partial Y_{tr}}{\partial v} = \frac{\partial \left(\rho (\Omega R)^2 \pi R^2 C_T^{tr}\right)}{\partial v}$$
$$\frac{\partial C_T^{tr}}{\partial v} = \frac{a_{tr}\sigma_{tr}}{2}\left(\frac{1}{2}\left(\frac{\partial \mu_{ztr}}{\partial v} - \frac{\partial \lambda_0^{tr}}{\partial v}\right)\right) \qquad (4\text{-}27)$$
$$\frac{\partial \mu_{ztr}}{\partial v} = \frac{1}{\Omega_{tr} R_{tr}}$$
$$\frac{\partial \lambda_0^{tr}}{\partial v} = \frac{\dfrac{C_{Tt} a \sigma}{2\Omega_{tr} R_{tr}} - \dfrac{8\lambda_{0T}^2 (\mu_{ZT} - \lambda_{0T})}{\Omega_{tr} R_{tr}}}{8\lambda_{0T}(\mu_T^2 + (\mu_{ZT} - \lambda_{0T})^2) - 8\lambda_{0T}^2 (\mu_{ZT} - \lambda_{0T}) + C_{Tt} a \sigma / 2}$$

$$\frac{\partial L_{vf}}{\partial v} = \frac{\partial \left(-0.5\rho S_{vf} (C_{L\alpha}^{vf} V_\infty^{tr} + |\, v_{vf}\,|) v_{vf}\right)}{\partial v} h_{tr}$$
$$\frac{\partial L_{vf}}{\partial v} = (-0.5\rho S_{vf} (C_{L\alpha}^{vf} V_\infty^{tr} + |\, v_{vf}\,|) - 0.5\rho S_{vf}\, sign(v_{vf}) v_{vf}) h_{tr} \qquad (4\text{-}28)$$
$$v_{vf} = v - \varepsilon_{vf}^{tr} V_{itr} - l_{tr} r$$
$$w_{tr} = w + l_{tr} q - K_\lambda V_{imr}$$

The directional stability derivative N_v is critically important for both static and dynamic stability of helicopters. The main contributors are the tail rotor, and the vertical fin.

$$\frac{\partial N}{\partial v} = \frac{\partial (-Q_e + N_{vf} + N_{tr})}{\partial v}$$
$$\frac{\partial Q_e}{\partial v} = \rho (\Omega R)^2 \pi R^3 \frac{\partial C_Q}{\partial v}$$
$$\frac{\partial C_Q}{\partial v} = \frac{\partial C_T}{\partial v}(\lambda_0 - \mu_z) + C_T\left(\frac{\partial \lambda_0}{\partial v}\right) + \frac{C_{D0}\sigma}{8}\left(\frac{7}{3} * 2 * \mu * \frac{\partial \mu}{\partial v}\right) \qquad (4\text{-}29)$$
$$\frac{\partial N_{vf}}{\partial v} = \frac{\partial (-Y_{vf} l_{tr})}{\partial v} = -l_{tr} \frac{\partial Y_{vf}}{\partial v}$$
$$\frac{\partial N_{tr}}{\partial v} = \frac{\partial (-Y_{tr} l_{tr})}{\partial v} = -l_{tr} \frac{\partial Y_{tr}}{\partial v}$$

4.2.1.4 Heave Damping Z_w

The main rotor dominates the heave damping derivative and the thrust coefficient derivative is used to approximate the heave damping in Eq. (4-30).

$$Z_w = -\frac{\rho(\Omega R)\pi R^2}{M_a}\frac{\partial C_T}{\partial \mu_z} \tag{4-30}$$

$$C_T = \frac{a_0 s}{2}\left[\theta_0\left(\frac{1}{3}+\frac{\mu^2}{2}\right)+\frac{\mu_z-\lambda_0}{2}\right] \tag{4-31}$$

$$\lambda_0 = \frac{C_T}{2\eta_w\sqrt{\left[\mu^2+(\lambda_0-\mu_z)^2\right]}} \tag{4-32}$$

By using the linear aerodynamics view, the thrust coefficient is proportional to the normal velocity component, μ_z; however the induced inflow will change if the vertical velocity is perturbed in the following way.

$$\frac{\partial C_T}{\partial \mu_z} = \left(\frac{\partial C_T}{\partial \mu_z}\right)_{\lambda=0} + \frac{\partial C_T}{\partial \lambda}\frac{\partial \lambda}{\partial \mu_z} = \frac{a_0 s}{4}\left(1-\frac{\partial \lambda}{\partial \mu_z}\right) \tag{4-33}$$

Good approximations for heave damping in hover and forward velocity flight are as [1].

$$\frac{\partial C_T}{\partial \mu_z} = \frac{2a_0 s\lambda_0}{16\lambda_0 + a_0 s} \tag{4-34}$$

4.2.1.5 Control Derivatives Z_{θ_0} and $Z_{\delta_{lon}}$

The derivative of thrust with main rotor collective and longitudinal cyclic can be obtained from the thrust and uniform inflow equations [1].

Approximations for hover and forward flight can be written as

$$\begin{aligned} \frac{\partial C_T}{\partial \theta_0} &\approx \frac{8}{3}\left(\frac{a_0 s\lambda_0}{16\lambda_0 + a_0 s}\right) & \frac{\partial C_T}{\partial \theta_0} &\approx \frac{4}{3}\left(\frac{a_0 s\mu\left(1+1.5\mu^2\right)}{8\mu + a_0 s}\right) \\ Z_{\theta_0} &\approx \frac{8}{3}\frac{a_0 A_b \rho(\Omega R)^2 \lambda_0}{\left(16\lambda_0 + a_0 s\right)M_a} & Z_{\theta_0} &\approx -\frac{4}{3}\frac{a_0 A_b \rho\left(\Omega R\right)^2 \mu}{\left(8\mu + a_0 s\right)M_a}\left(1+1.5\mu^2\right) \end{aligned} \tag{4-35}$$

The thrust change with longitudinal cyclic is zero in the hover and the approximation for forward flight can be written as

$$\frac{\partial C_T}{\partial \delta_{lon}} \approx \frac{2a_0 s\mu^2}{8\mu + a_0 s} \qquad Z_{\delta_{lon}} = \frac{-2a_0 A_b \rho\left(\Omega R\right)^2 \mu^2}{\left(8\mu + a_0 s\right)M_a} \tag{4-36}$$

4.2.2 Numeric Linearization

Numeric linearization is performed by introducing deviations to the control inputs and states from the trim points. The derivatives are obtained by using the Eq. (4-37)

$$X_u = \frac{X(u+\Delta u) - X(u)}{\Delta u} \tag{4-37}$$

The performances of numerical and analytical linearization are tested by the nonlinear model at the trim point. Small control deviations from the trim control points are introduced to each of the linear model and the nonlinear model. The procedure is given in Figure 4-4. The trajectories of the states are observed in a time interval. The linearization results of the forward flight are shown Figure 4-5.

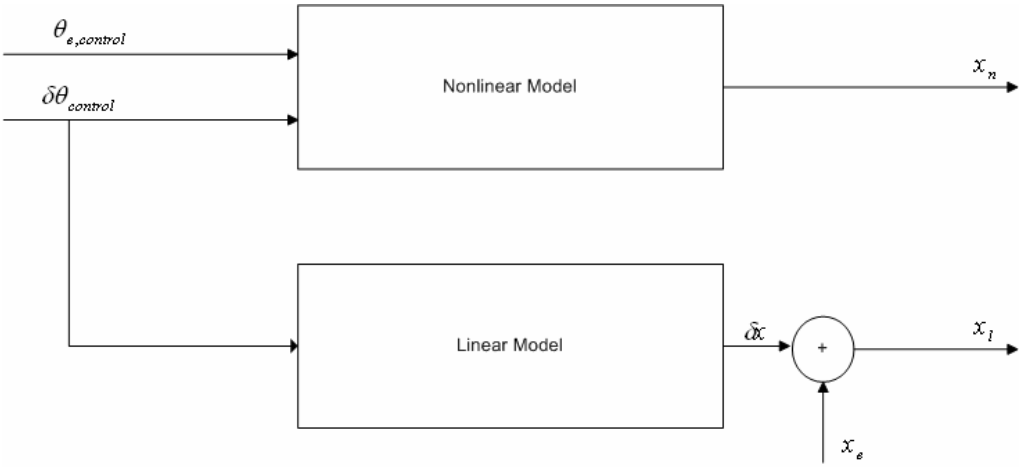

Figure 4-4 Comparison of nonlinear and linear model at trim point

From Figure 4-5 and Figure 4-6, the performance of the linear model created by the numerical linearization has a better performance then the linear model created by the analytical linearization for representing the nonlinear model. The states of the numerical linear model are on top of the states of the nonlinear model.

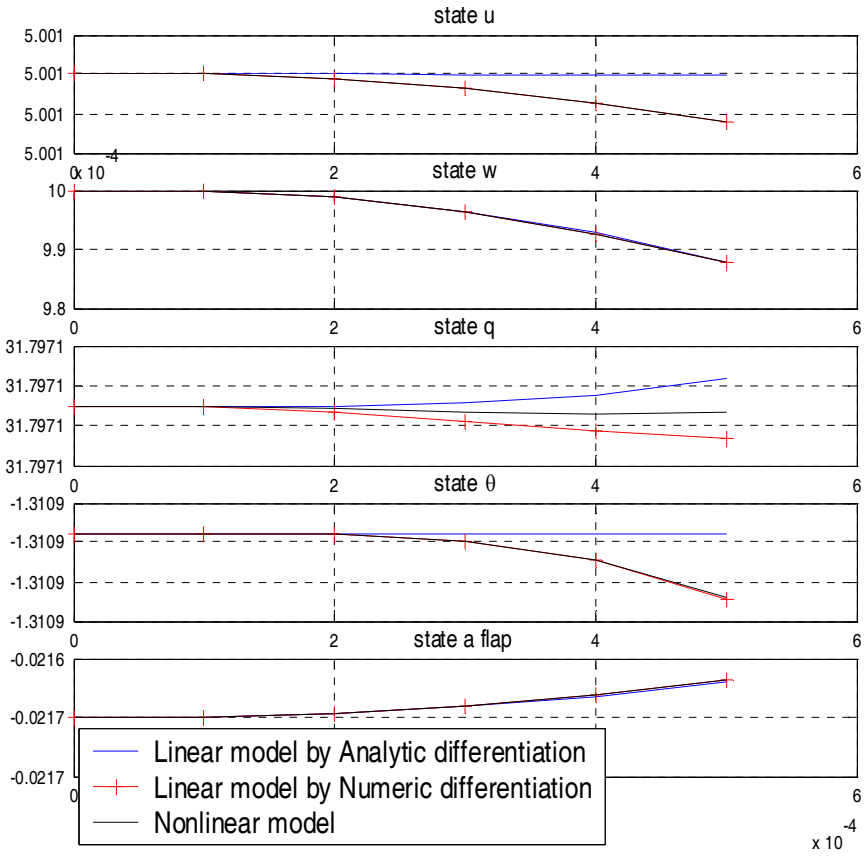

Figure 4-5 Linearization at forward flight longitudinal states

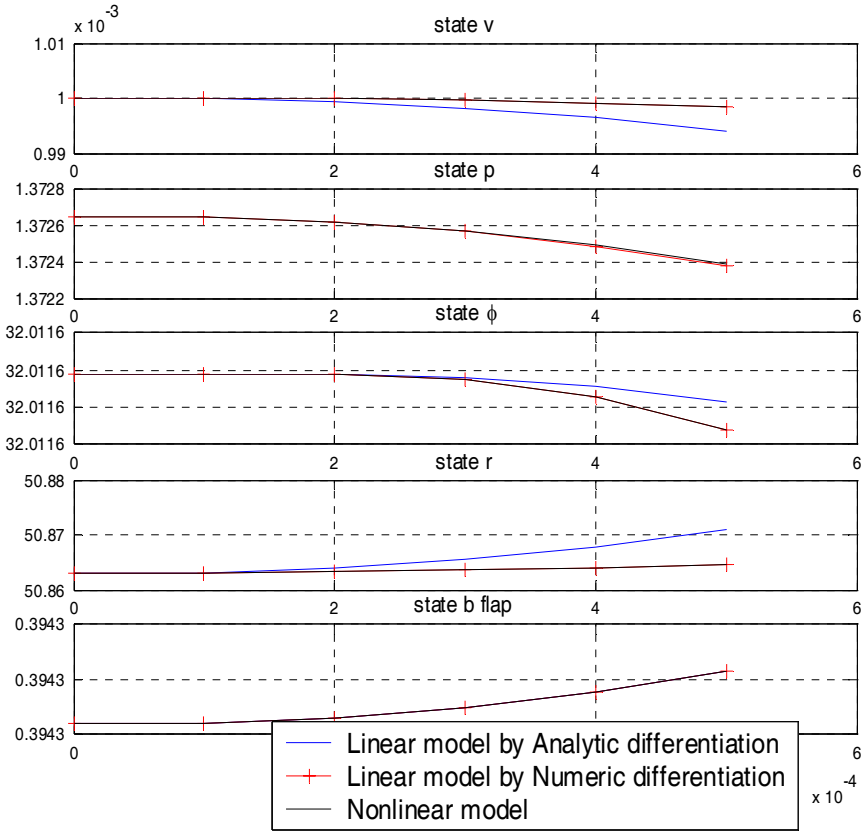

Figure 4-6 Linearization at forward flight lateral states

4.3 Conclusions

The linearization and trim algorithms are presented in this section. Linearization is made at the trim point in order to control the states by linear controller. The residual forces and moments will be effective at points other then the trim points. Hence, before linearization the trim process is implemented. Linearization is based on the Taylor series expansion of the external forces and moments. The external forces and moments are the linear functions of the perturbed states around the trim point if the perturbations are small. The numeric and analytic linearization methods are implemented. The performances of the methods are tested by introducing small perturbations to the control inputs. The results of the numerical linearization method, $\mathbf{A}$ and $\mathbf{B}$ matrices, appears to be a better approximation for nonlinear

helicopter model at trim points. As a conclusion, the linear control design techniques can be used to control the helicopter.

CHAPTER 5

AUTOPILOT DESIGN

There are classical methods utilized for the flight control of the unmanned helicopters [5]. These methods are implemented by using the sequential loop closures. In the inner loop, the controller stabilizes the fast dynamics such as rotational rates of the helicopter. The inner loops can be designed by classical methods such as PID [5]. The slow dynamics are controlled by the outer loops. These loops can be designed by the root locus method. The classical successive-loop-closure approach means that the control gains are selected individually. This design procedure becomes difficult when there is multi input, multi output, or multiple feedback loops [7].

Linear quadratic regulator (LQR) is a linear approach of modern control techniques that provides sufficient gain and phase margins. By this approach, once the performance criterion is selected the control gains are computed simultaneously. Moreover, the stability margins are guaranteed. In this thesis, LQR approach is implemented for flight control system. The linear model obtained at the trim point in chapter IV is used for the control design. An integrator is introduced in order to solve the tracking problem. The linear model can be presented as

$$\begin{aligned} \dot{\mathbf{x}} &= \mathbf{A}\mathbf{x} + \mathbf{B}\mathbf{u} \\ \mathbf{y} &= \mathbf{C}\mathbf{x} \end{aligned} \tag{5-1}$$

Since the non-linear model is changing between the different flight regimes the control gains that are computed for the different flight regimes are gain-scheduled.

5.1 Gain Scheduling

Gain scheduling is a popular approach to control nonlinear plants. The main idea behind the gain scheduling is to use linear controller design techniques to design a parameter-dependent controller for a nonlinear plant. The first step in gain scheduling is to linearize the nonlinear model at one or more operating points (trim points) which cover the range of the plant's dynamics. Then linear design methods are applied to the linearized model at each operating point in order to arrive a set of linear feedback control laws that perform satisfactorily when the closed-loop system is operated near the respective operating points. The final step is the actual gain scheduling, which is interpolating the linear control law designs at intermediate trim points [23]. The scheme is to divide the nonlinear system into linear systems using a scheduling variable and control the nonlinear system by interpolating the gains using the current value of the scheduling variable designed for linear systems. The fundamental issue is to select the scheduling variable. The basic guideline for selection of the scheduling variable is that the scheduling variable should capture the plant the nonlinearities [24].

$$\mathbf{x} = \mathrm{f}(\mathbf{x}, \mathbf{u}) \tag{5-2}$$

The linear models used for approximation of the nonlinear model shown in Eq. (5-2) are constructed at each trim point as in Eq. (5-3).

$$\begin{aligned} \dot{\mathbf{x}}_\delta(t) &= \mathbf{A}(\sigma_i)\mathbf{x}_\delta(t) + \mathbf{B}(\sigma_i)\mathbf{u}_\delta(t) \\ \mathbf{y}_\delta(t) &= \mathbf{C}(\sigma_i)\mathbf{x}_\delta(t) \end{aligned} \tag{5-3}$$

where

$$
\begin{aligned}
\mathbf{A}(\sigma_i) &= \frac{\partial \mathrm{f}(\mathbf{x}_e(\sigma_i), \mathbf{u}_e(\sigma_i))}{\partial \mathbf{x}} \\
\mathbf{B}(\sigma_i) &= \frac{\partial \mathrm{f}(\mathbf{x}_e(\sigma_i), \mathbf{u}_e(\sigma_i))}{\partial \mathbf{u}} \\
\mathbf{x}_\delta(t) &= \mathbf{x}(t) - \mathbf{x}_e(\sigma) \\
\mathbf{u}_\delta(t) &= \mathbf{u}(t) - \mathbf{u}_e(\sigma) \\
\mathbf{y}_\delta(t) &= \mathbf{y}(t) - \mathbf{y}_e(\sigma)
\end{aligned}
\tag{5-4}
$$

The interpretation is that at each fixed σ linearization shown in Eq. (5-3) describes the local behavior of the nonlinear plant about the equilibrium (trim) point [24]. The corresponding control laws for each linear model are shown by applying state feedback control.

$$
\mathbf{u}_\delta(\sigma_i) = -\mathbf{K}(\sigma_i)\mathbf{x}_\delta(\sigma_i) \tag{5-5}
$$

The gain-scheduling variable for this study is chosen as the forward body velocity since the dynamics of the helicopter changes significantly through hover to forward flight. The feedback gains computed in the next section are scheduled with the forward velocity.

5.2 LQR Design

Linear quadratic regulator (LQR) with full-state feedback minimizes the cost function in Eq. (5-6).

$$
J = \frac{1}{2}\int_0^\infty (\mathbf{x}\mathbf{Q}\mathbf{x}^{\mathrm{T}} + \mathbf{u}\mathbf{R}\mathbf{u}^{\mathrm{T}})dt \tag{5-6}
$$

where J is the performance index, $\mathbf{Q}$ and $\mathbf{R}$ are symmetric positive semi definite matrices called *weighting matrices*. The feedback gains that minimize the performance index subject to Eq. (5-1) is shown as in Eq. (5-7).

$$
\mathbf{u} = -\mathbf{K}\mathbf{x} \tag{5-7}
$$

where $\mathbf{K}$ is a matrix of the feedback gains. The $\mathbf{Q}$ and $\mathbf{R}$ matrices will be determined according to the requirements on time-domain criterions (settling time, rise time) and control effort.

The solution for the regulator problem is solved as transforming the dynamical optimization into static one, which is easier to solve. Suppose there is a symmetric, positive-semi definite matrix $\mathbf{P}$ such that

$$\frac{\mathbf{d}}{\mathbf{dt}}(\mathbf{x}^{\mathbf{T}}\mathbf{P}\mathbf{x}) = -\mathbf{x}^{\mathbf{T}}(\mathbf{Q} + \mathbf{K}^{\mathbf{T}}\mathbf{R}\mathbf{K})\mathbf{x} \tag{5-8}$$

then J, the performance index can be written as

$$J = \frac{1}{2}\mathbf{x}^{\mathbf{T}}(\mathbf{0})\mathbf{P}\mathbf{x}(\mathbf{0}) - \frac{\mathbf{1}}{\mathbf{2}}\lim_{\mathbf{t}\to\infty}\mathbf{x}^{\mathbf{T}}(t)\mathbf{P}\mathbf{x}(t) \tag{5-9}$$

Under the asymptotically stable closed-loop assumption, J becomes

$$J = \frac{1}{2}\mathbf{x}^{\mathbf{T}}(\mathbf{0})\mathbf{P}\mathbf{x}(\mathbf{0}) \tag{5-10}$$

The closed-loop system can be written using Eq. (5-1) and Eq. (5-7) as

$$\dot{\mathbf{x}} = (\mathbf{A} - \mathbf{B}\mathbf{K})\mathbf{x} = \mathbf{A}_{\mathbf{c}}\mathbf{x} \tag{5-11}$$

The Eq. (5-8) becomes

$$-\mathbf{x}^{\mathbf{T}}(\mathbf{Q} + \mathbf{K}^{\mathbf{T}}\mathbf{R}\mathbf{K}) = \dot{\mathbf{x}}^{\mathbf{T}}\mathbf{P}\mathbf{x} + \mathbf{x}^{\mathbf{T}}\mathbf{P}\dot{\mathbf{x}} = \mathbf{x}^{\mathbf{T}}(\mathbf{A}_{\mathbf{c}}^{\mathbf{T}}\mathbf{P} + \mathbf{P}\mathbf{A}_{\mathbf{c}})\mathbf{x} \tag{5-12},$$

This equivalence must hold for every initial condition. Hence, it can be written as

$$\mathbf{g} = \mathbf{A}_{\mathbf{c}}^{\mathbf{T}}\mathbf{P} + \mathbf{P}\mathbf{A}_{\mathbf{c}} + \mathbf{K}^{\mathbf{T}}\mathbf{R}\mathbf{K} + \mathbf{Q} = 0 \tag{5-13}$$

So the optimization problem can be stated as to find the feedback gains $\mathbf{K}$ that minimizes J in Eq. (5-10) subject to Eq. (5-11). The Lagrange multiplier approach is used to solve this optimization. The Hamiltonian is

$$H = \frac{1}{2}\mathbf{x}^{\mathrm{T}}(\mathbf{0})\mathbf{P}\mathbf{x}(\mathbf{0}) + \mathbf{g}\mathbf{S} \tag{5-14}$$

where $\mathbf{S}$ is a symmetric matrix of Lagrange multipliers. The necessary conditions are

$$\begin{aligned}
\mathbf{0} &= \frac{\partial H}{\partial \mathbf{S}} = \mathbf{g} = \mathbf{A}_{\mathbf{c}}^{\mathbf{T}}\mathbf{P} + \mathbf{P}\mathbf{A}_{\mathbf{c}} + \mathbf{K}^{\mathbf{T}}\mathbf{R}\mathbf{K} + \mathbf{Q} \\
\mathbf{0} &= \frac{\partial H}{\partial \mathbf{P}} = \mathbf{A}_{\mathbf{C}}\mathbf{S} + \mathbf{S}\mathbf{A}_{\mathbf{c}}^{\mathbf{T}} + \mathbf{x}(\mathbf{0}) \\
\mathbf{0} &= \frac{1}{2}\frac{\partial H}{\partial \mathbf{K}} = \mathbf{R}\mathbf{K}\mathbf{S} - \mathbf{B}\mathbf{P}\mathbf{S}
\end{aligned} \tag{5-15}$$

If $\mathbf{R}$ is positive definite then the feedback gains can be obtained as

$$\mathbf{K} = \mathbf{R}^{-1}\mathbf{B}^{\mathbf{T}}\mathbf{P} \tag{5-16}$$

So it is not necessary to solve for $\mathbf{S}$ to obtain the feedback gains. This result and the combining of the Eq. (5-11) and Eq. (5-14) will yield

$$\mathbf{0} = \mathbf{A}^{\mathbf{T}}\mathbf{P} + \mathbf{P}\mathbf{A} + \mathbf{Q} - \mathbf{P}\mathbf{B}\mathbf{R}^{-1}\mathbf{B}^{\mathbf{T}}\mathbf{P} \tag{5-17}$$

called Algebraic Riccati Equation (ARE). Solving the ARE will be sufficient to compute the feedback gains by the relation in Eq. (5-17). There are various tools for solving ARE. MATLAB is used to solve the ARE in this study.

5.2.1 Tracking with LQR

LQR is used to regulate the states through zero. On the other hand, in the tracking problem the states should go to the desired values from their initial values. By augmenting integral actions to the LQR it is possible to track the desired values. For this purpose an error state is defined as

$$e = x_{com} - x \tag{5-18}$$

Let

$$\xi = \begin{bmatrix} \dot{x} \\ e \end{bmatrix} \tag{5-19}$$

then

$$\dot{\xi} = \begin{bmatrix} \ddot{x} \\ \dot{e} \end{bmatrix} = \begin{bmatrix} A & 0 \\ -1 & 0 \end{bmatrix} \begin{bmatrix} \dot{x} \\ e \end{bmatrix} + \begin{bmatrix} B \\ 0 \end{bmatrix} v \tag{5-20}$$

where

$$v = \dot{u} \tag{5-21}$$

Using the results of the previous section the control law v will be

$$v = -\begin{bmatrix} K_1 & K_2 \end{bmatrix} \begin{bmatrix} \dot{x} \\ e \end{bmatrix} \tag{5-22}$$

and

$$u = \int v = -K_1 x - \int K_2 e \tag{5-23}$$

By this control law the LQR will regulate the error state e through zero which is needed for tracking. The overshoot, rise-time can be controlled by the weighting matrix $\mathbf{Q}$.

5.2.2 Longitudinal Autopilot Design

The helicopter dynamics can be separated into two decoupled dynamics for low advance ratio ($\mu < 0.15$) [4]. The longitudinal-vertical and lateral-directional dynamics are decoupled; hence, the feedback controllers are decoupled.

The longitudinal-vertical perturbations from the trim values are $\delta \mathbf{x}^T = \begin{bmatrix} \delta u & \delta w & \delta q & \delta\theta & \delta a_1 \end{bmatrix}$. The first five rows of the $\mathbf{A}$ matrix in Eq. (4-17) is used for this autopilot design. The commanded variables are u and $\dot{h}$. By defining the errors as

$$\begin{aligned} e_{11} &= u_{com} - u \\ e_{12} &= \dot{h}_{com} - h \end{aligned} \tag{5-24}$$

where u_{com} is body-fixed frame forward velocity command and $\dot{h}_{com}$ is Earth-fixed reference frame altitude rate command, where the altitude rate is

$$\dot{h} = -u\sin(\theta) + w\cos(\theta)\cos(\phi) + u_e\cos(\theta_e)\theta \tag{5-25}$$

assuming v side velocity is zero. The augmented system becomes

$$\begin{bmatrix} \ddot{u} \\ \ddot{w} \\ \ddot{q} \\ \ddot{\theta} \\ \ddot{a}_1 \\ \dot{e}_{11} \\ \dot{e}_{12} \end{bmatrix} = \begin{bmatrix} X_u & X_w - q_e & X_q - w_e & X_\theta - g\cos(\theta_e) & X_{a_1} & 0 & 0 \\ Z_u + q_e & Z_w & Z_q + u_e & Z_\theta - g\cos(\phi_e)\sin(\theta_e) & Z_{a_1} & 0 & 0 \\ M_u & M_w & M_q & M_\theta & M_{a_1} & 0 & 0 \\ 0 & 0 & \cos(\phi_e) & 0 & 0 & 0 & 0 \\ 0 & 0 & -1 & 0 & -1/\tau & 0 & 0 \\ -1 & 0 & 0 & 0 & 0 & 0 & 0 \\ \sin(\theta_e) & -\cos(\theta_e)\cos(\phi_e) & 0 & u_e\cos(\theta_e) & 0 & 0 & 0 \end{bmatrix} \begin{bmatrix} \dot{u} \\ \dot{w} \\ \dot{q} \\ \dot{\theta} \\ \dot{a}_1 \\ e_{11} \\ e_{12} \end{bmatrix} + \begin{bmatrix} X_{\delta_{lon}} & X_{\delta_\theta} \\ Z_{\delta_{lon}} & Z_{\delta_\theta} \\ M_{\delta_{lon}} & M_{\delta_\theta} \\ 0 & 0 \\ A_{lon} & 0 \\ 0 & 0 \\ 0 & 0 \end{bmatrix} v$$

where

$$v = \dot{u} = \begin{bmatrix} \dot{\delta}_{lon} \\ \dot{\delta}_{\theta} \end{bmatrix} \tag{5-26}$$

The solution found in the previous section is used to compute the feedback gains. The ratio of the magnitude of the weighting matrices $\mathbf{Q}$ and $\mathbf{R}$ is the key element in designing the controller. Some ratios and the corresponding step responses of the linear system are shown in Figure 5-1. The system becomes quicker when the ratio gets larger. However, the control effort becomes larger. That is shown in Figure 5-2.

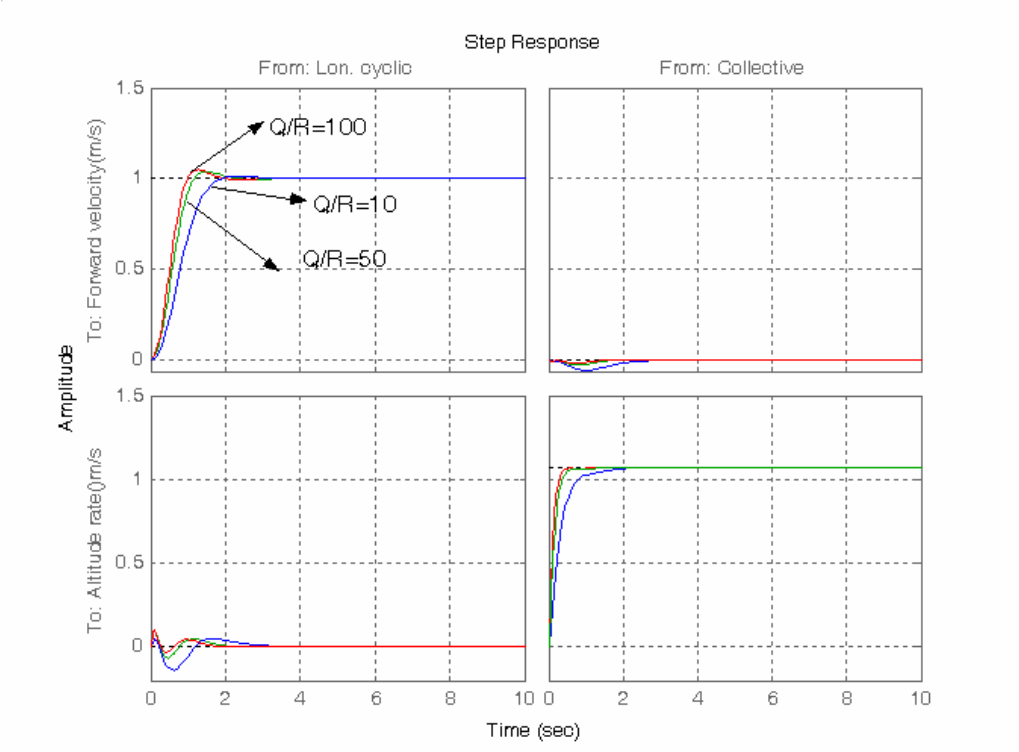

Figure 5-1 Step response with different weighting matrices

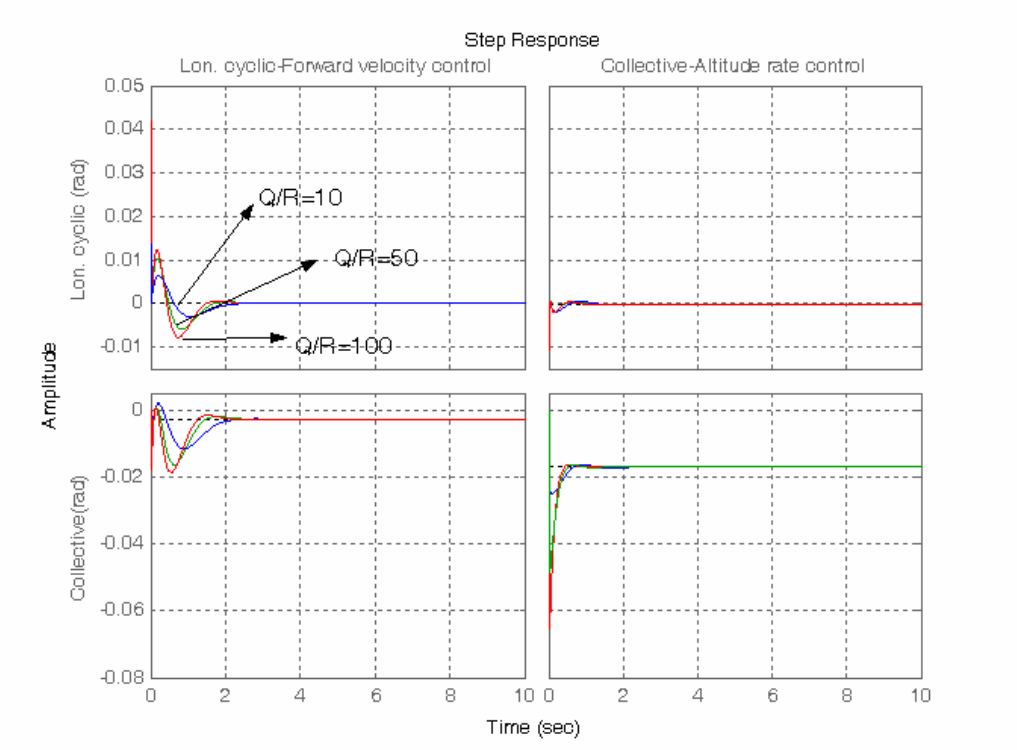

Figure 5-2 Control inputs with different $\mathbf{Q/P}$ parameters

The gains are computed at forward velocities of -3, 0, 3, 6, 9, 12 and 15m/s of body-fixed frame. Then scheduling of gains according to the forward velocity is implemented.

The control architecture is shown in Figure 5-3.

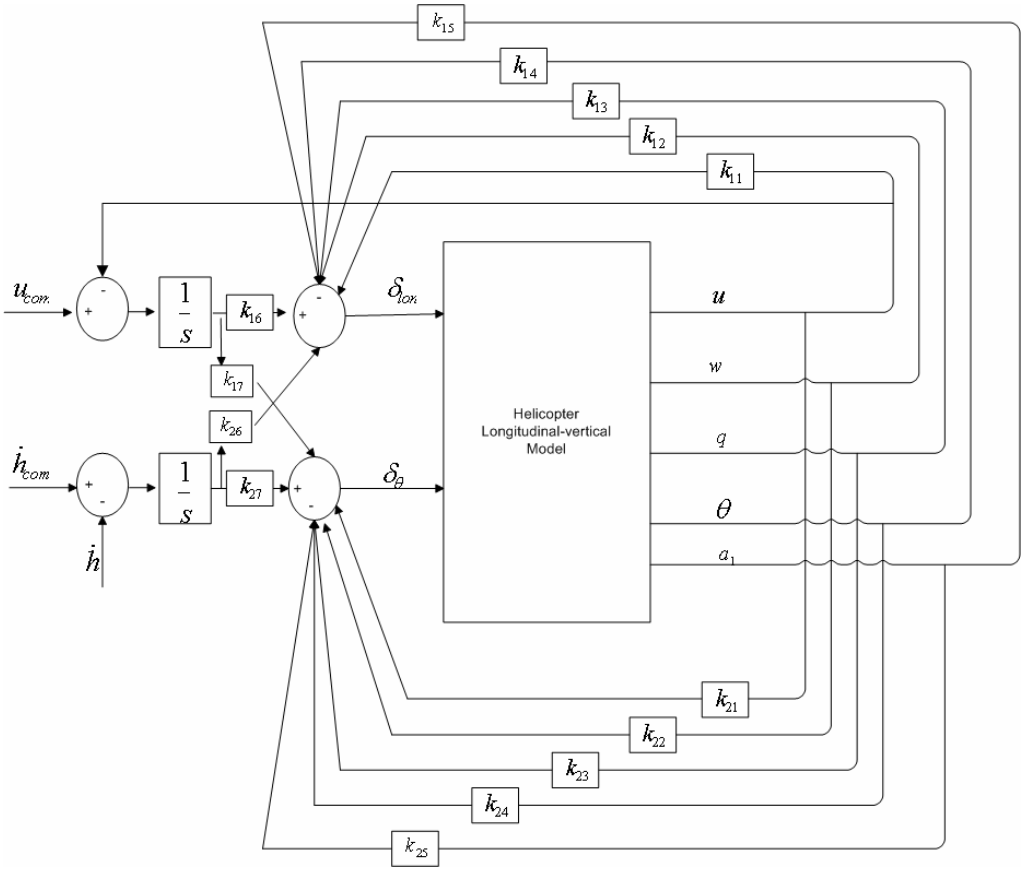

Figure 5-3 Longitudinal-vertical autopilot architecture

5.2.2.1 Altitude Control

The attitude control is implemented as an outer loop around the altitude rate controller. The altitude controller is a proportional controller and the proportional gain is found by the root-locus method. The gains are also scheduled with the forward velocity. The controller architecture is shown in Figure 5-4.

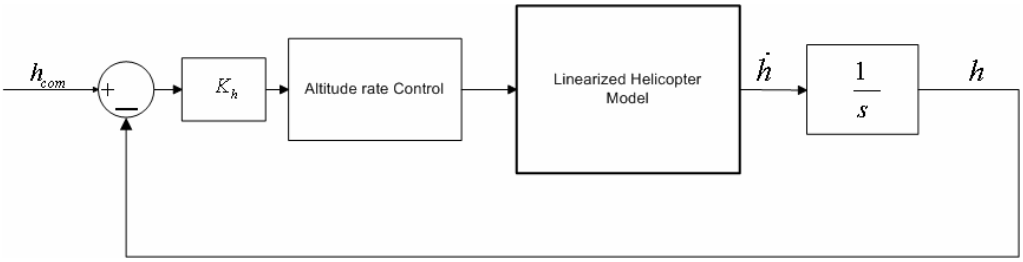

Figure 5-4 The altitude controller architecture

The root-locus of the altitude rate controller for 6 m/s forward velocity is shown in Figure 5-5.

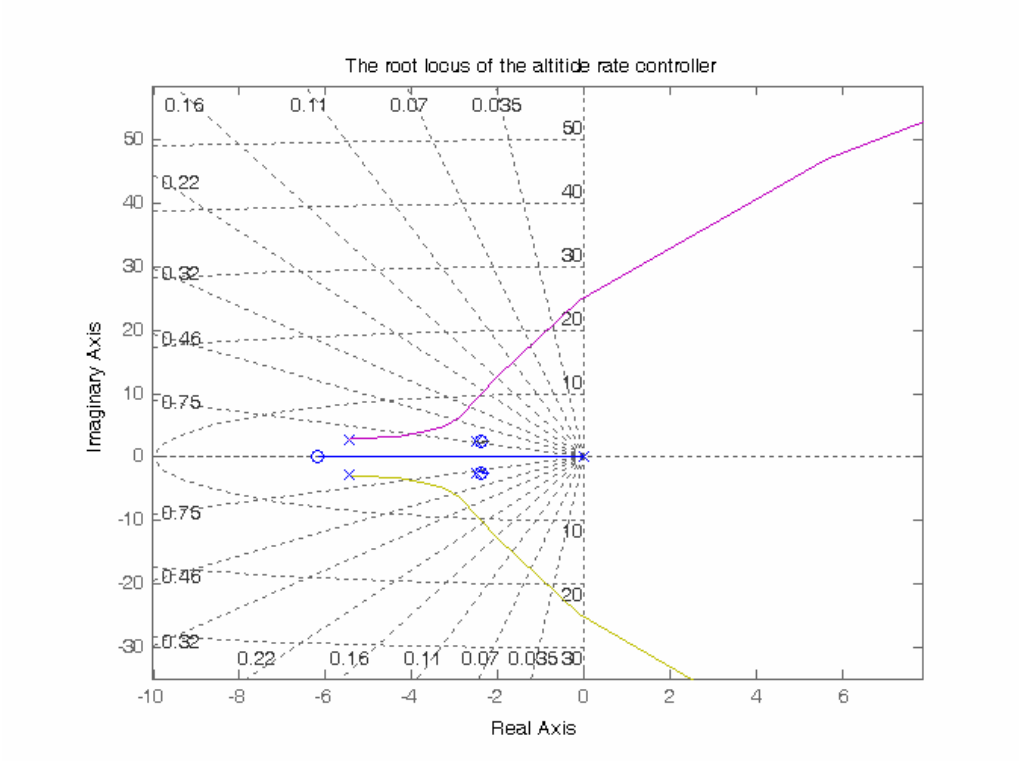

Figure 5-5 The root locus of the altitude rate controller

5.2.3 Lateral Autopilot Design

The same guidelines are used for the lateral-directional autopilot. The perturbations from the trim states are $\delta\mathbf{x} = \begin{bmatrix} \delta v & \delta p & \delta\phi & \delta r & \delta b_1 \end{bmatrix}$. The second set of five rows of the $\mathbf{A}$ matrix in Eq. (4-17) is used for this autopilot design. The commanded variables are v and r. By defining the errors as

$$\begin{aligned} e_{21} &= v_{com} - v \\ e_{22} &= r_{com} - r \end{aligned} \tag{5-27}$$

where v_{com} is body-fixed frame side velocity command and r_{com} is the yaw rate of the helicopter. The bank -to-turn coordinated maneuver is realized by commanding the yaw rate r. Then this command is projected to the bank angle ϕ, because $v_{com} = 0$, so the helicopter banks.

The augmented system becomes

$$\begin{bmatrix} \ddot{v} \\ \ddot{p} \\ \ddot{\phi} \\ \ddot{r} \\ \ddot{b}_1 \\ \ddot{e}_{21} \\ \ddot{e}_{22} \end{bmatrix} = \begin{bmatrix} Y_v & Y_p + w_e & Y_\phi + g\cos(\phi_e)\cos(\theta_e) & Y_r - u_e & Y_{b_1} & 0 & 0 \\ L_v & L_p & L_\phi & L_r & L_{b_1} & 0 & 0 \\ 0 & 1 & 0 & 0 & 0 & 0 & 0 \\ N_v & N_p & N_\phi & N_r & N_{b_1} & 0 & 0 \\ 0 & 1 & 0 & 0 & 1/\tau & 0 & 0 \\ -1 & 0 & 0 & 0 & 0 & 0 & 0 \\ 0 & 0 & 0 & -1 & 0 & 0 & 0 \end{bmatrix} \begin{bmatrix} \dot{v} \\ \dot{p} \\ \dot{\phi} \\ \dot{r} \\ \dot{b}_1 \\ e_{21} \\ e_{22} \end{bmatrix} + \begin{bmatrix} Y_{\delta_{lat}} & Y_{\delta_{Tail}} \\ L_{\delta_{lat}} & L_{\delta_{Tail}} \\ 0 & 0 \\ N_{\delta_{lat}} & N_{\delta_{Tail}} \\ B_{lat} & 0 \\ 0 & 0 \\ 0 & 0 \end{bmatrix} \nu$$

where

$$\nu = \dot{u} = \begin{bmatrix} \dot{\delta}_{lat} \\ \dot{\delta}_{Tail} \end{bmatrix} \tag{5-28}$$

The step response of the closed loop linear system is shown in Figure 5-6.

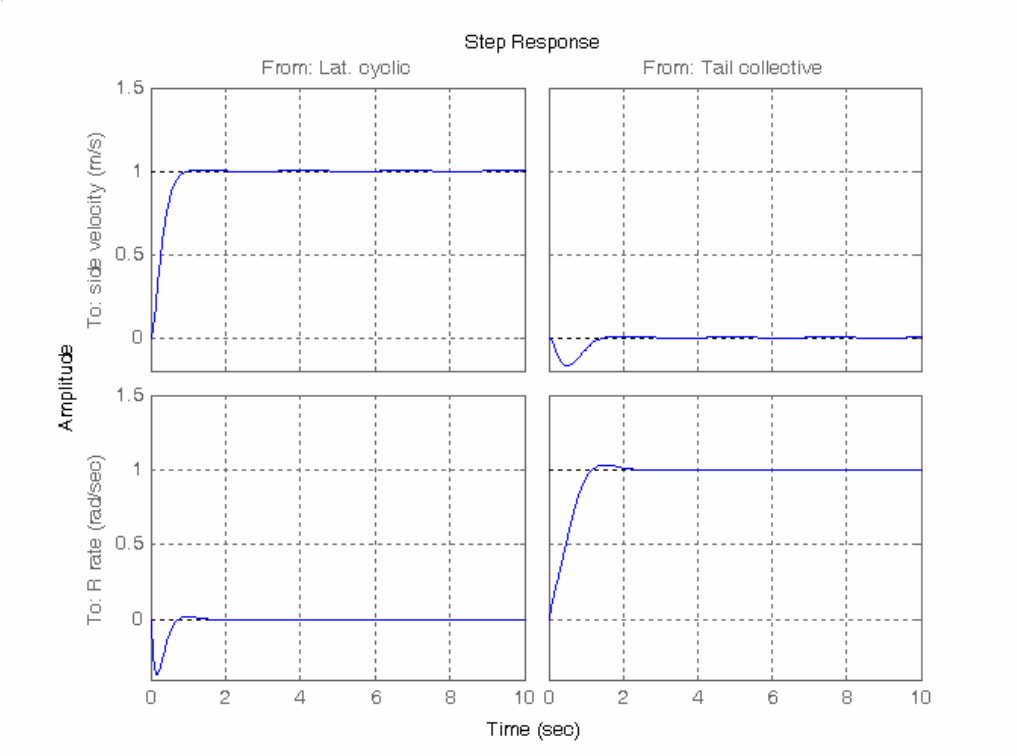

Figure 5-6 Step response of the lateral-directional autopilot

The control architecture is shown in Figure 5-7.

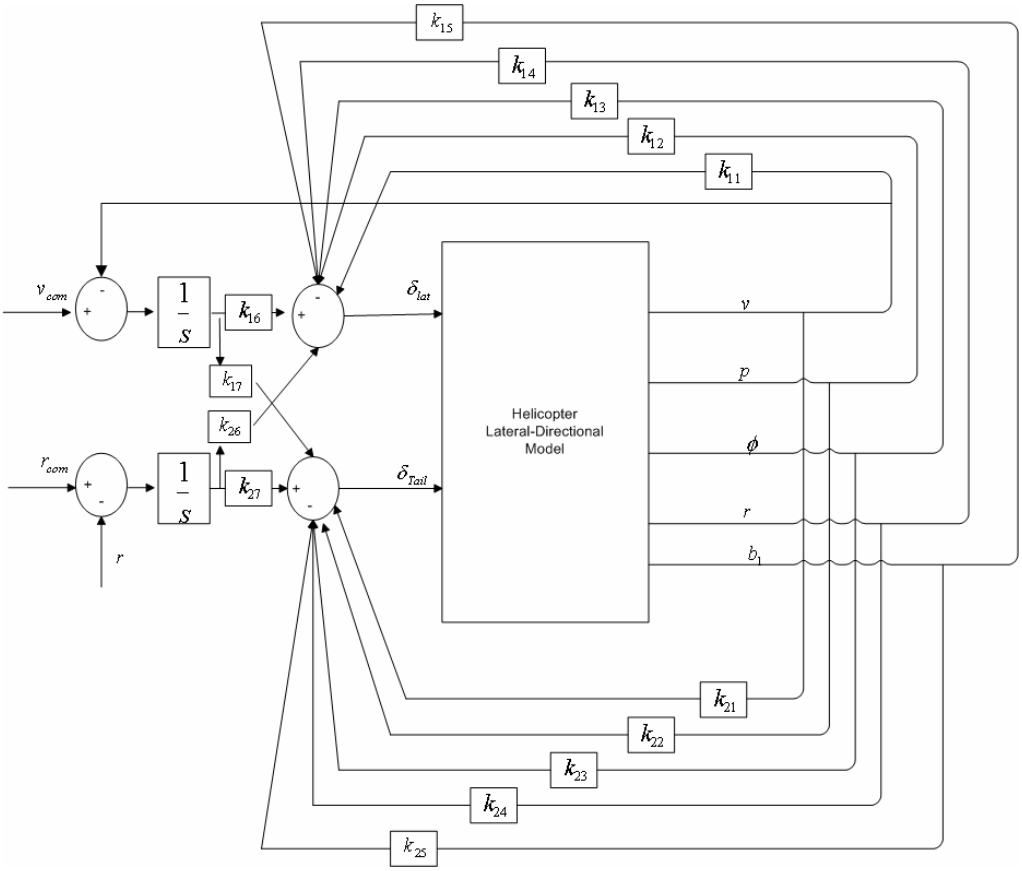

Figure 5-7 Lateral-directional autopilot architecture

In hover, the directional control is achieved by the tail control and in forward flight; the directional control is done by the lateral cyclic input. This is implemented by the gains k_{27} and k_{26} shown in Figure 5-7. These gains are scheduled by the forward velocity. The k_{27} gain is getting small in magnitude as the forward velocity increasing and the k_{26} gain gets larger. This is shown in Figure 5-8

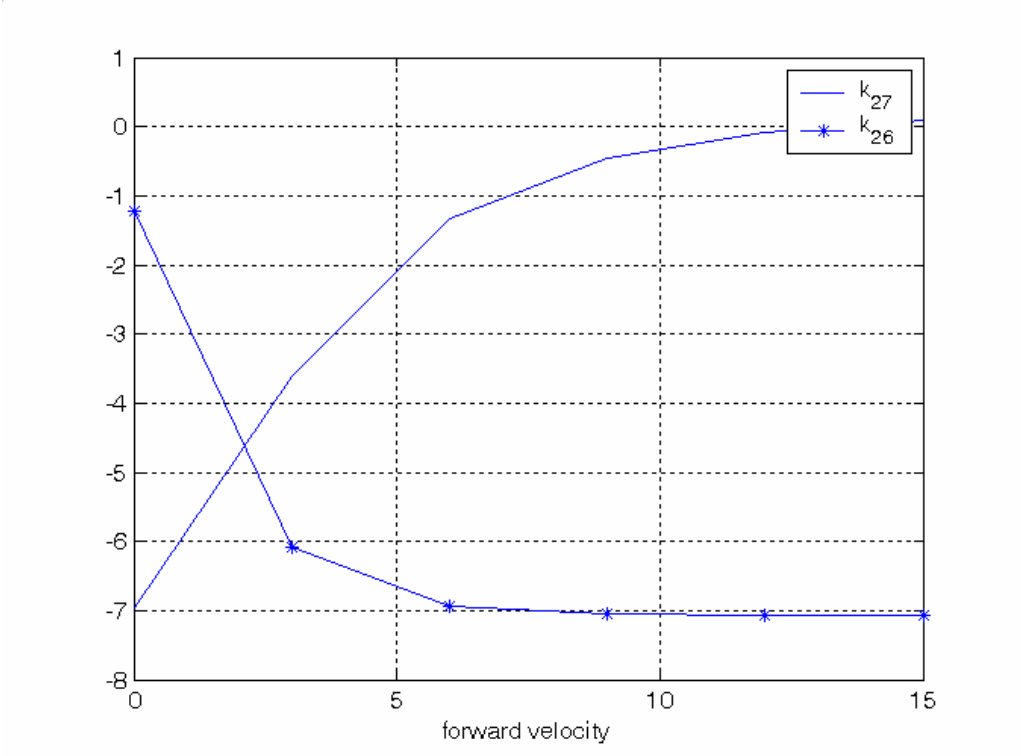

Figure 5-8 The heading control gains

5.2.3.1 Heading Control

The reference command to the lateral-directional controller is yaw rate command. In order to control the heading of the helicopter, an outer loop around the directional controller will be needed. The heading angle is assumed as in Eq. (5-25)

$$\dot{\psi} = r \tag{5-29}$$

The heading loop contains only a proportional gain. This gain is found by the root locus method. The control architecture is shown in Figure 5-9.

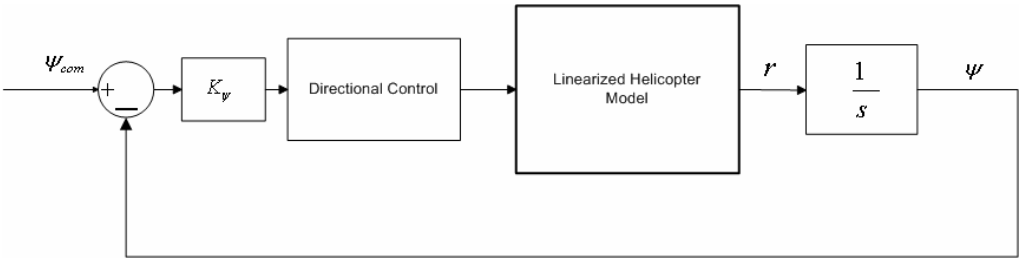

Figure 5-9 Heading control architecture

The root-locus of the directional controller for 6 m/s forward velocity is shown in Figure 5-10.

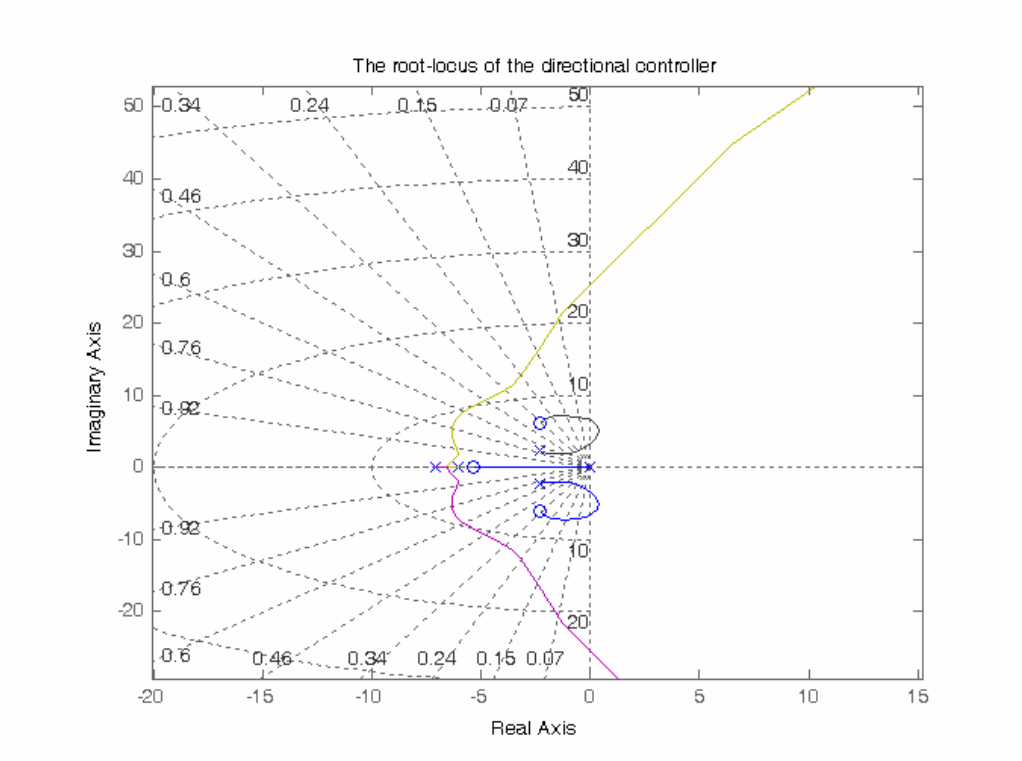

Figure 5-10 The root-locus of the directional controller

5.2.4 Command Filtering

The reference inputs for all the controllers are filtered. This filtering is necessary for fast input changes. The filters are second order filters with scheduling natural frequency with the forward velocity. The command and the filtered command are shown in Figure 5-11.

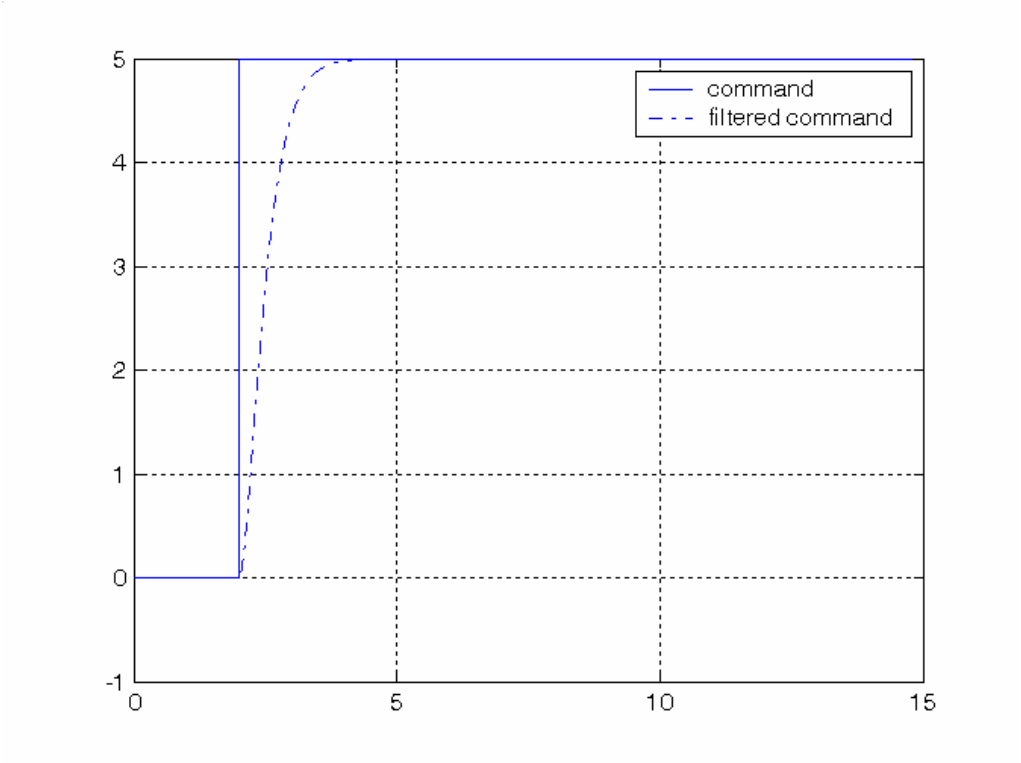

Figure 5-11 Command filter

5.3 Conclusions

In this chapter an LQR, based controller design technique is presented. The helicopter dynamics is separated into two decoupled dynamics. Longitudinal and lateral dynamics are used to design two separate controllers. The longitudinal controller features the body axis forward velocity u_{cmd} and altitude rate $\dot{h}_{cmd}$ as the command variables. The lateral controller features the body-axis side velocity

v_{cmd} and the yaw rate r_{cmd} a a command variables. In addition, the altitude h_{cmd} and heading angle ψ_{cmd} are used as command variables instead of altitude rate $\dot{h}_{cmd}$ and yaw rate r_{cmd} by augmenting proportional gains around the accompanying controllers. The controllers designed at various operating points, which cover the flight envelope. By using gain, scheduling a global controller is attained.

CHAPTER 6

GUIDANCE

Guidance is used to take the helicopter to the target position. The position and the angles received from an inertial measurement unit and from GPS are used for this aim. The target position can be moving throughout the flight or it can be stationary. The moving target position and the velocity information should be extracted from sensors like IR. After having all the information about the helicopter and the target position, guidance algorithm produces the commands that will be executed by the autopilots. In other words, autopilot realizes the commands of the guidance to reach the target. Therefore, the output of the guidance should be appropriate for the autopilot. This relation of the guidance and the autopilot is shown in Figure 6-1.

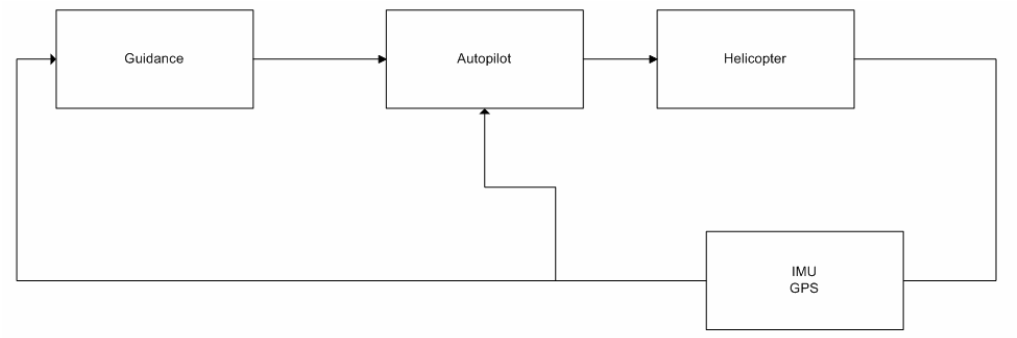

Figure 6-1 The guidance and control system

A general way to make an unmanned vehicle fly along a trajectory is to design the guidance algorithms in the horizontal and vertical planes separately. In such cases usually the horizontal guidance is often designed for threat avoidance, terrain

masking, achievement of desired attack direction, or arrival at the target location at a desired time, while vertical guidance is for terrain following or achievement of a height trajectory [11].

Waypoint guidance is common for cruising autonomous vehicles. Its task is to generate references for the autopilots of the vehicle by using the waypoints. The waypoints are given in a order to form a desired trajectory. A waypoint is defined by its position (x_i , y_i , z_i). The path between two waypoints is not necessarily specified by the user. A waypoint is reached when the vehicles arrives to a sufficiently small distance of the waypoint. The next waypoint is activated whenever the vehicle reaches the previous waypoint in the sense described above. Such a guidance method can be remarkably robust to disturbances and other unanticipated events. On the other hand, waypoint guidance cannot give tight path control [12].

6.1 Basic Line of Sight Guidance Algorithm

The autopilot designed in the previous chapter tracks the heading angle, forward velocity, altitude rate and side velocity. The side velocity is kept zero through the cruise. The forward velocity command is the desired velocity at the target. The heading angle and the altitude rate commands are generated according to the target and the helicopter position besides the velocity of the helicopter. Basic line of sight guidance is described by [16]. The algorithm provides a reference heading ψ_r which would guide the vehicle from its current position (x_c , y_c , z_c) towards the current waypoint (x_i , y_i , z_i). The reference heading for the horizontal plane is

$$\psi_i = a\tan(\frac{y_i - y_c}{x_i - x_c}) \qquad (6\text{-}1)$$

The reference heading in Eq (6-1) is computed by the four quadrant inverse tangent.

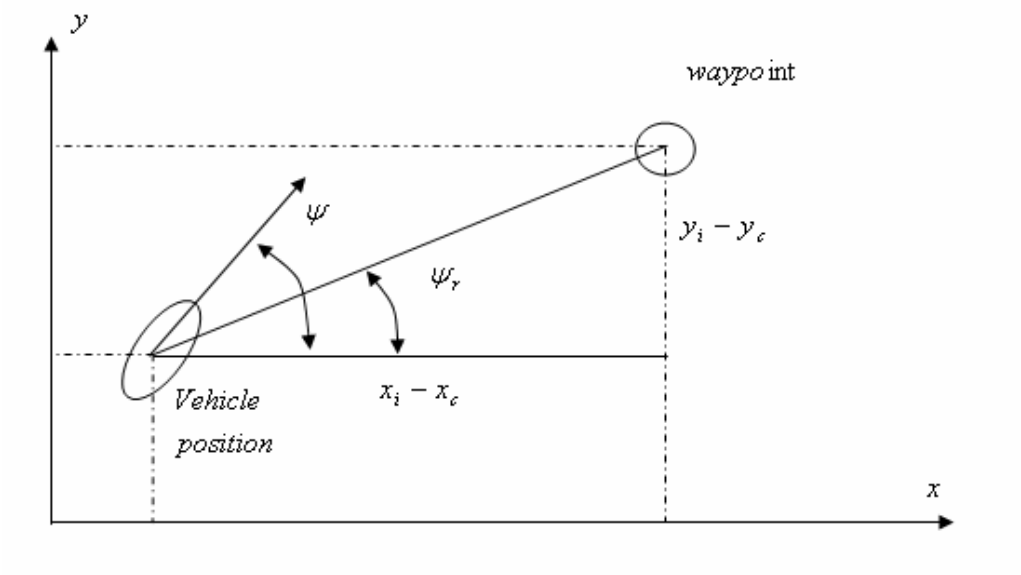

Figure 6-2 Reference heading for horizontal plane

In the vertical plane, the desired altitude is determined by the active waypoint. Achieving desired waypoint can be possible by lining the flight path angle with line of sight. Therefore, the desired flight path angle is

$$\lambda_i = a\tan(\frac{z_i - z_c}{x_i - x_c}) \tag{6-2}$$

The velocity components of the velocity in Earth-fixed reference frame is

$$\begin{aligned} \dot{x} &= V\cos(\gamma)\cos(\eta) \\ \dot{y} &= V\cos(\gamma)\sin(\eta) \\ \dot{z} &= -V\sin(\gamma) \end{aligned} \tag{6-3}$$

Using Eq (6-3) one can get flight path angle as

$$\gamma = a\tan(-\frac{\dot{z}}{\dot{x}}\cos(\eta)) \tag{6-4}$$

The desired $\dot{z}$ is computed by equating Eqns (6-2) and (6-4).

$$\dot{z}_d = -\dot{x}(\tan(\lambda_i))/\cos(\eta) \tag{6-5}$$

where η is the heading angle since the side velocity is zero.

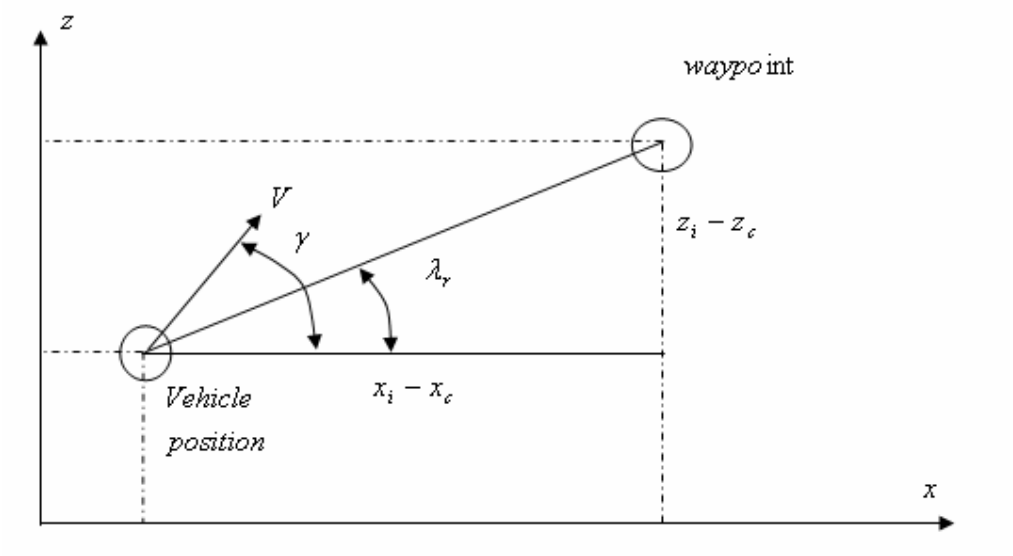

Figure 6-3 Reference flight path angle

The waypoint is reached when the vehicle lies within a circle of acceptance with a radius ρ around the waypoint. Resultant trajectories corresponding to two different radia of acceptance are shown in Figure 6-4 and Figure 6-5. The overshoot after turning is decreased when the radius of acceptance gets larger. There are smoothing algorithms to decrease the overshoots while resulting in larger turns [12], [17]. The radius of acceptance of a waypoint may be determined according to the turn radius to smooth the turns. The turn radius is given in [18] as

$$R = \frac{V^2}{g\tan(\phi)} \tag{6-6}$$

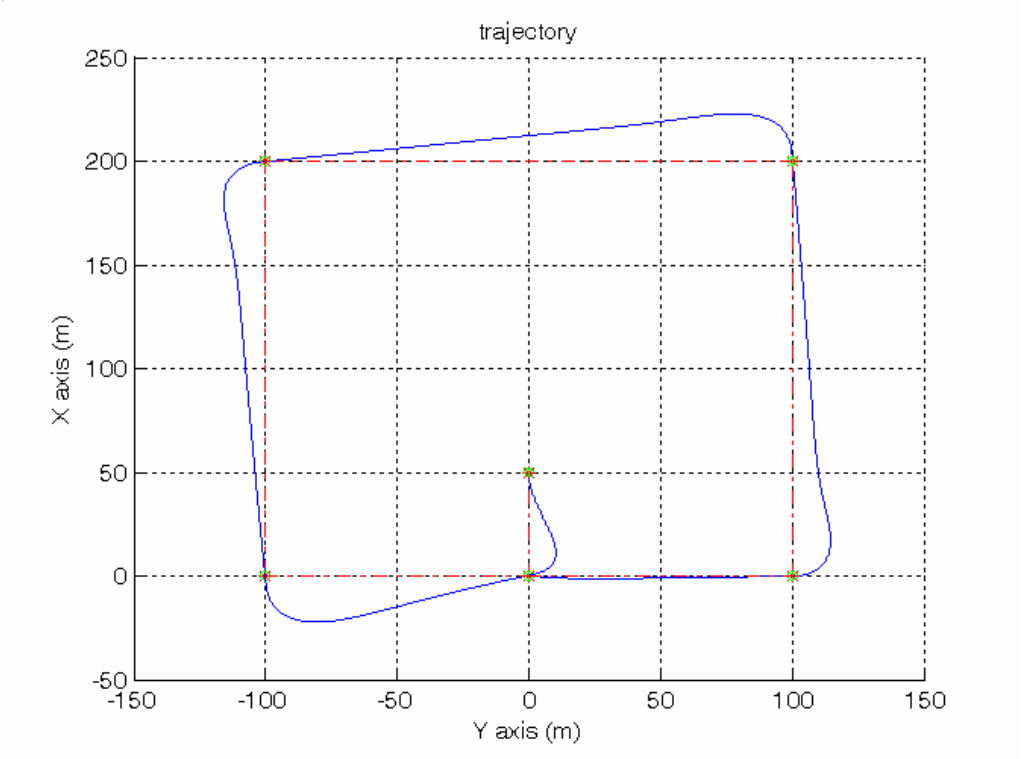

Figure 6-4 The 2m radius of acceptance

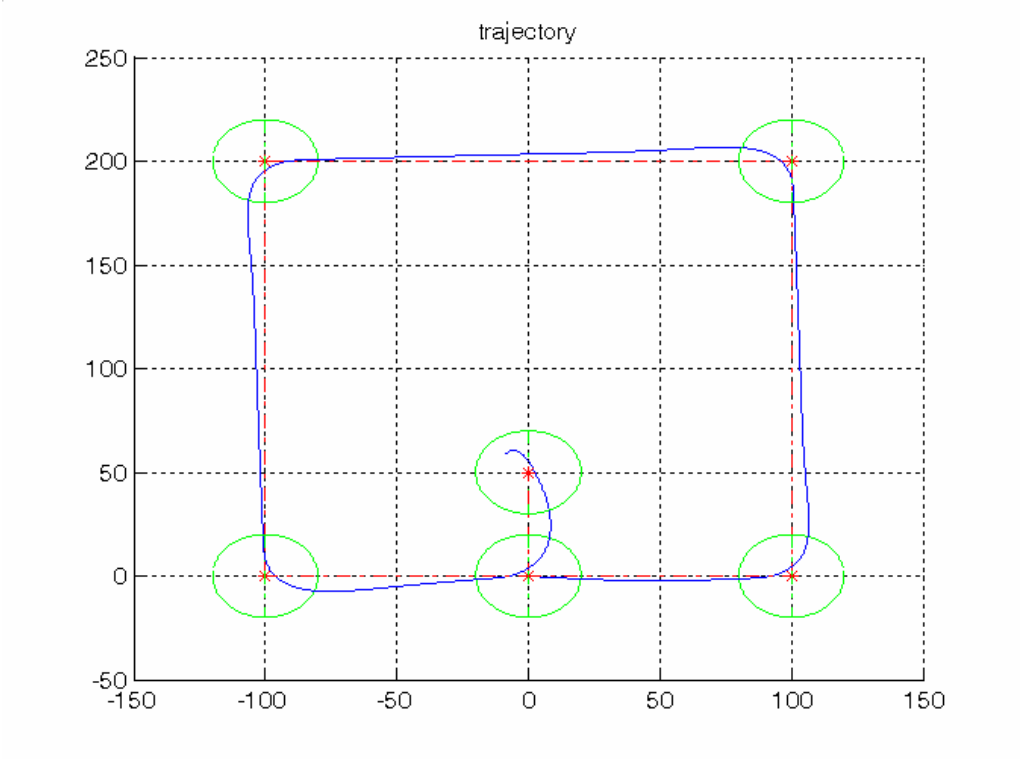

Figure 6-5 The 20m radius of acceptance

The desired trajectory and the helicopter trajectory formed by the waypoints extracted from the desired trajectory is given in Figure 6-8.

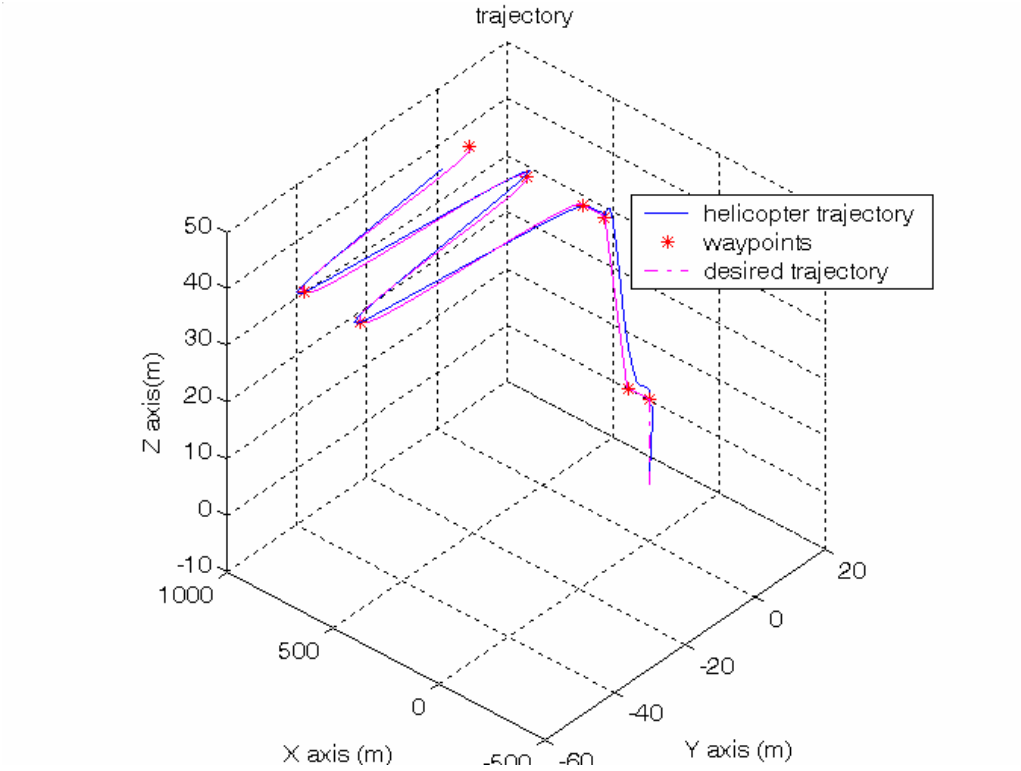

Figure 6-6 The desired and the helicopter trajectory

6.2 Missed Waypoint Detection

A waypoint is the called missed waypoint if the vehicle passes the waypoint radius of acceptance. Disturbances can cause the vehicle to skip a waypoint or the maneuverability of the vehicle may not be enough to manage to get to the waypoint. In such a case, to reroute the vehicle to the waypoint requires extra energy and time. Hence, the missed waypoint is discarded. The range between the vehicle and the waypoint is used to determine the missed waypoint detection. The range between the vehicle and the waypoint should decrease in order to approach the waypoint. A waypoint is missed if the range starts to increase.

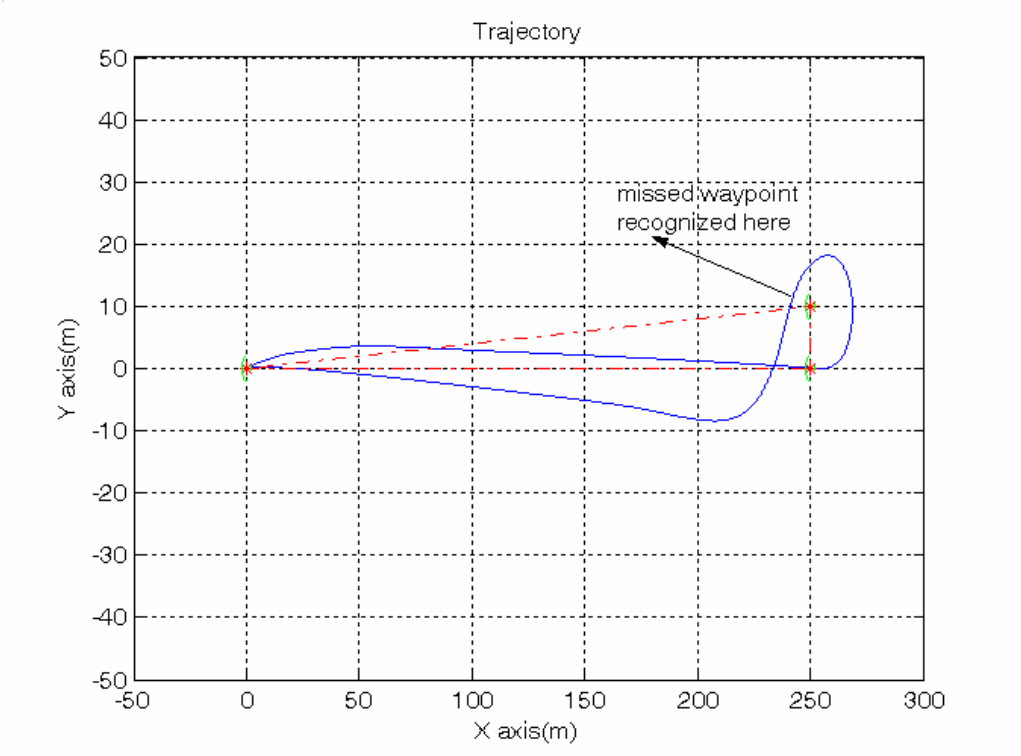

Figure 6-7 The missed waypoint

6.3 Non-stationary Waypoint Guidance

The non-stationary waypoint guidance is very much like the stationary waypoint guidance. A moving waypoint is used for guiding the vehicle. In other words, the vehicle tracks the moving waypoint. Usually the helicopter makes some shortcuts since the moving waypoint cruises ahead of the vehicle. The trajectories of the moving waypoint and the vehicle are given in Figure 6-8.

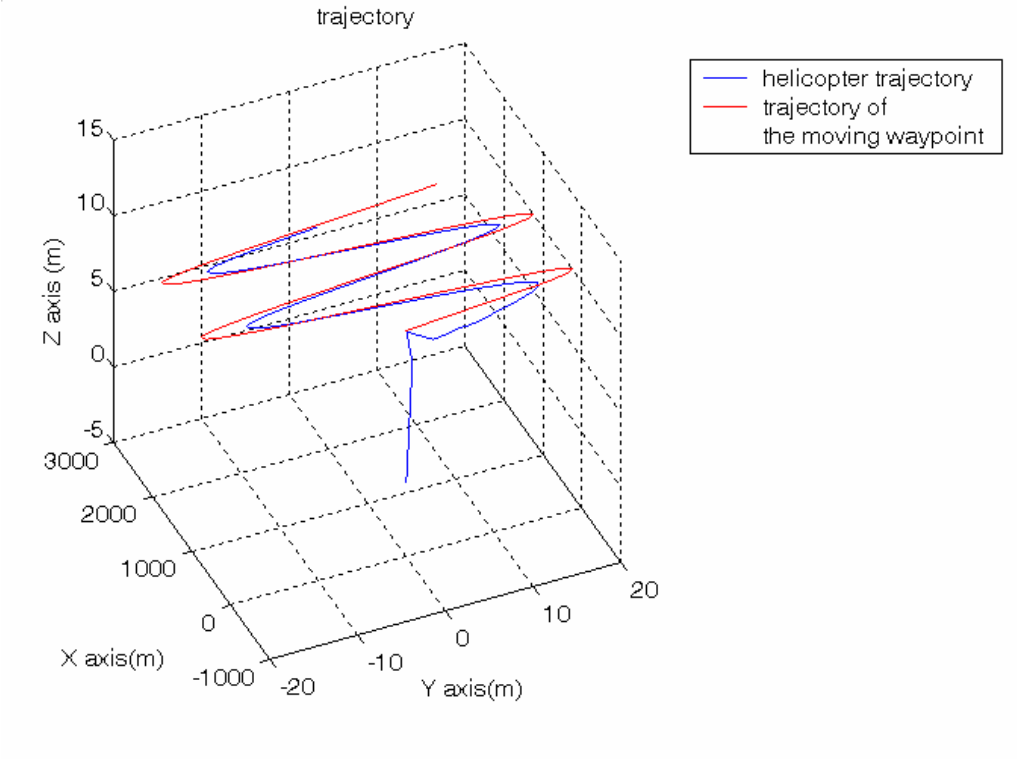

Figure 6-8 The moving waypoint trajectory

6.4 Conclusions

In this section, a waypoint guidance algorithm is presented. Waypoints are defined by their positions and the desired velocities at the waypoints. A sequence of waypoints is used for approximating a path. The active waypoint is used by the guidance as a target position. The next waypoint is activated when the previous waypoint is reached and the sequence will end up with a trajectory. The horizontal and vertical planes are separated. In the horizontal plane, the reference-heading angle is generated for the heading controller. The line-of sight is used as a heading angle command in order to direct the helicopter toward the active waypoint. In vertical plane, the reference altitude rate is generated. The direction of the velocity vector in the vertical plane, flight path angle, is aligned with the line of sight. The altitude rate controller is switched to the altitude controller if the altitudes of the successive waypoints are same.

CHAPTER 7

RESULTS

The performances of the guidance and autopilots are presented in this chapter. To measure the performances of the guidance and autopilot a test trajectory is chosen. Sharp turns are good examples to evaluate the performance of the autopilot since all the states change simultaneously. The waypoints given in Figure 7-1 are used as a test scenario. The body rates are shown in Figure 7-2. The ascending maneuver is the first 12sn.

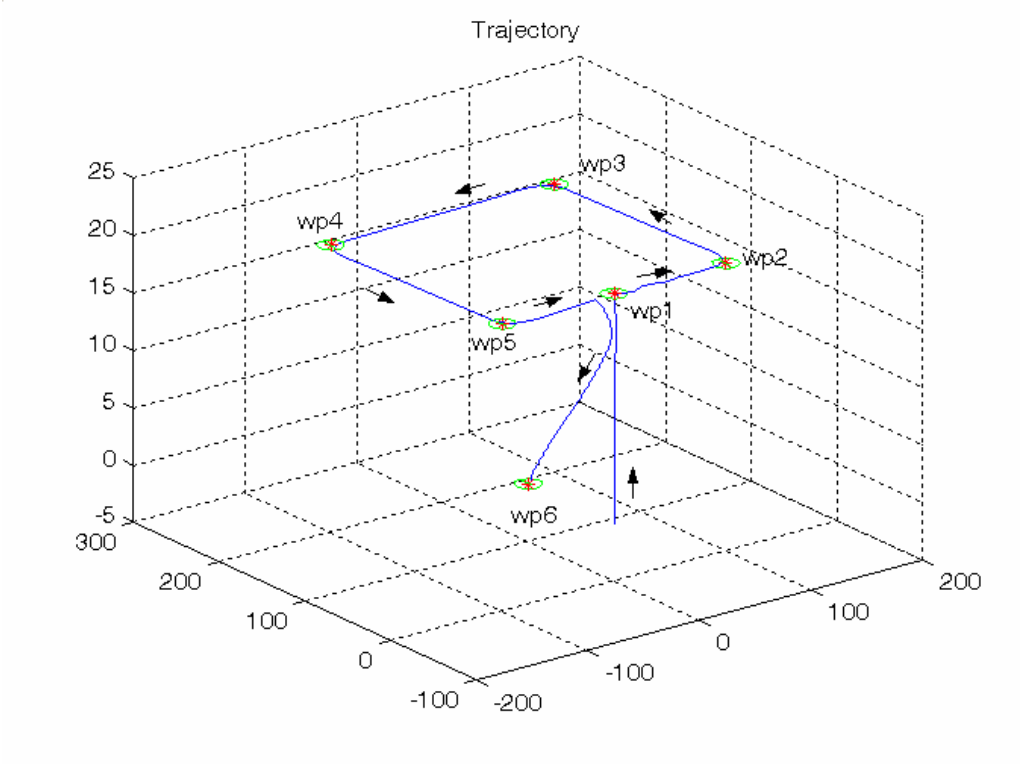

Figure 7-1Test trajectory

During this maneuver, the velocity controllers are active beside the heading controller. The altitude controller raises the helicopter to the vicinity of the desired altitude while the forward and side velocities and heading are kept as zero. After attaining sufficient altitude, the velocity controllers switch to position controllers in order to hold the helicopter at the desired position. The helicopter hovers about 2 sec. The first turn is the tail turn since the forward velocity is zero. After the tail turn, the forward velocity starts to increase shown in Figure 7-4 because of the commanded velocity at the second waypoint (wp2).

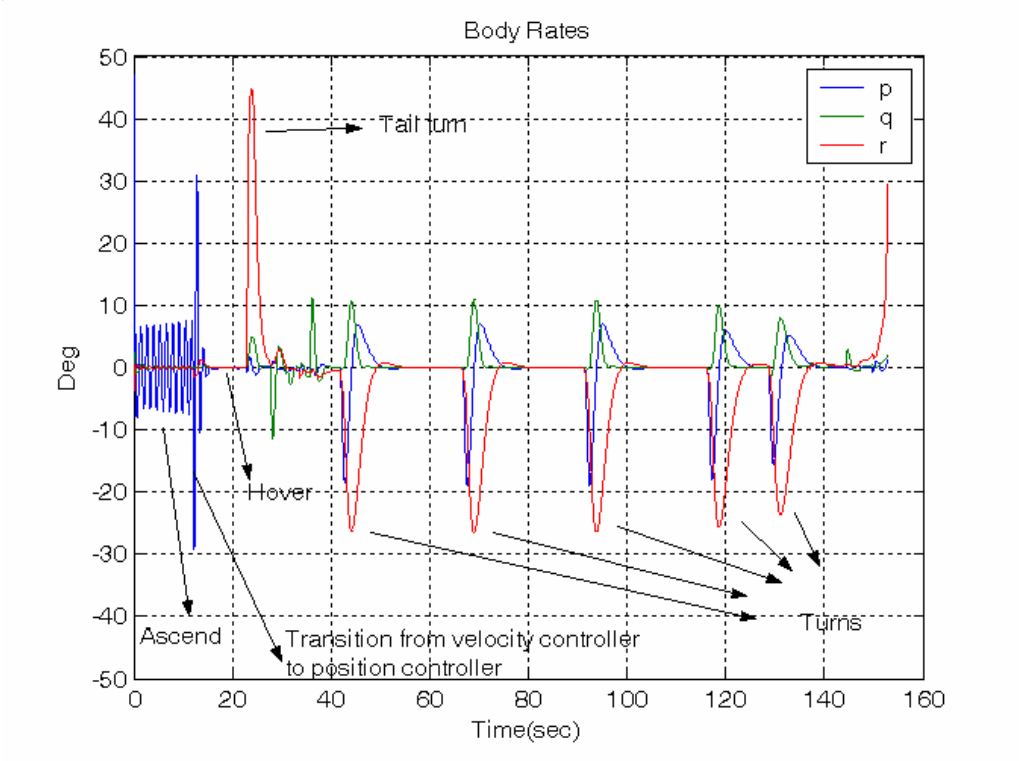

Figure 7-2 Body rates

The helicopter banks at every turn except the tail turn. This is shown in Figure 7-3. The theta angle converges to the trim value after the forward velocity settles to the stead-state value. Finally, the controller outputs are shown in Figure 7-5.

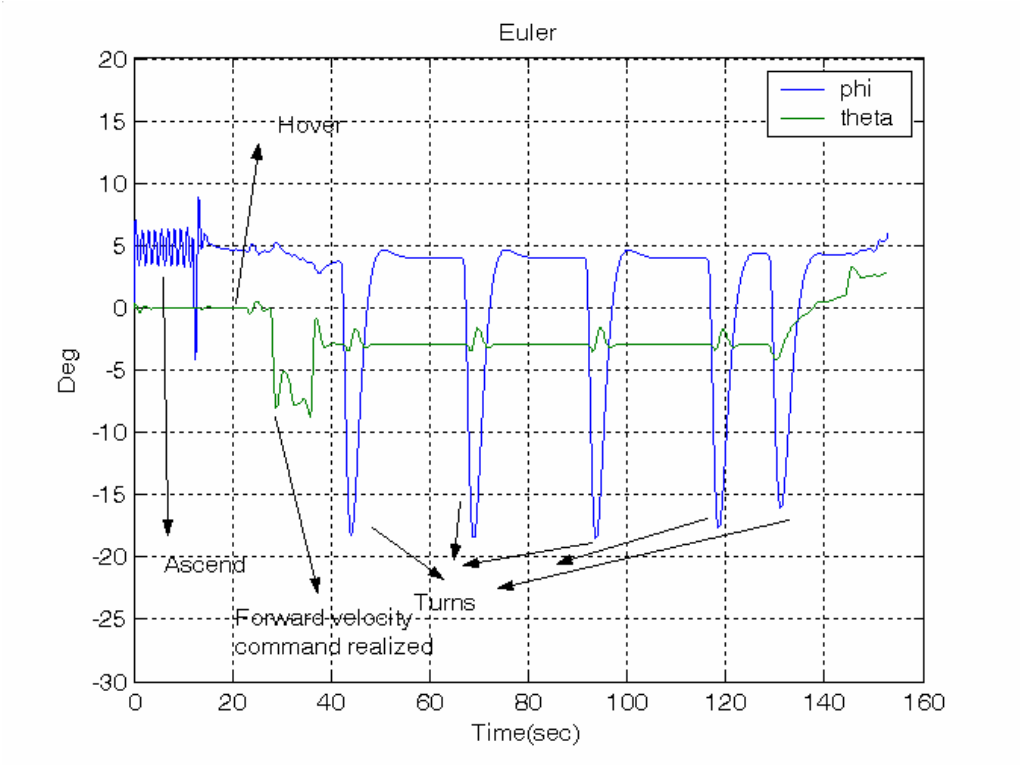

Figure 7-3 Euler angles

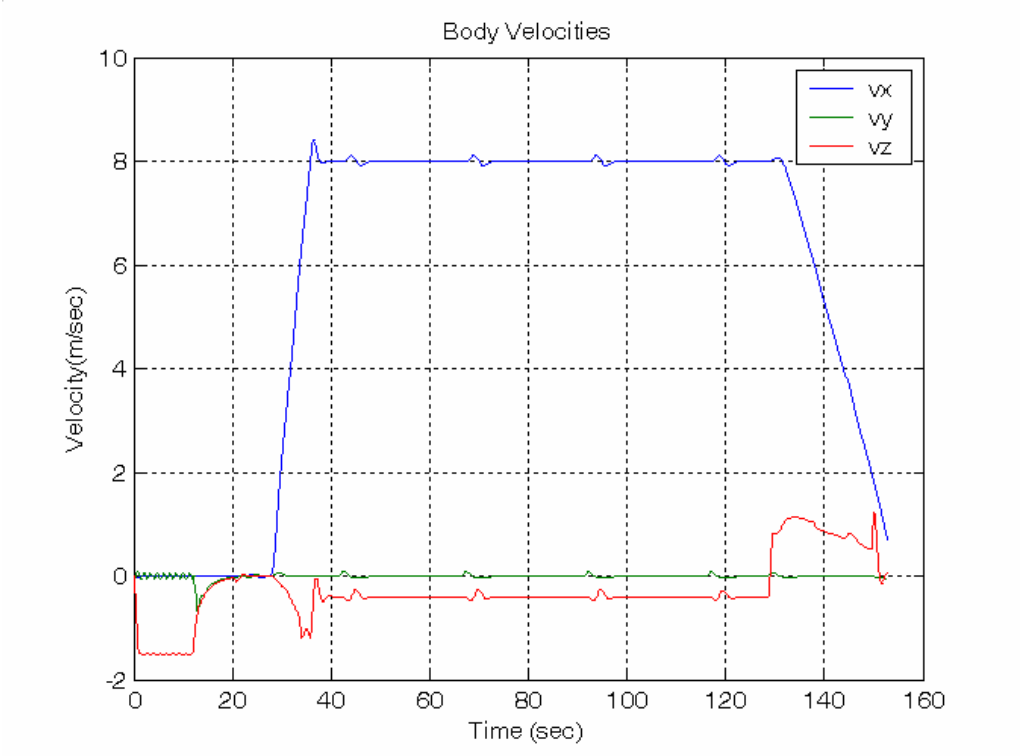

Figure 7-4 Body velocities

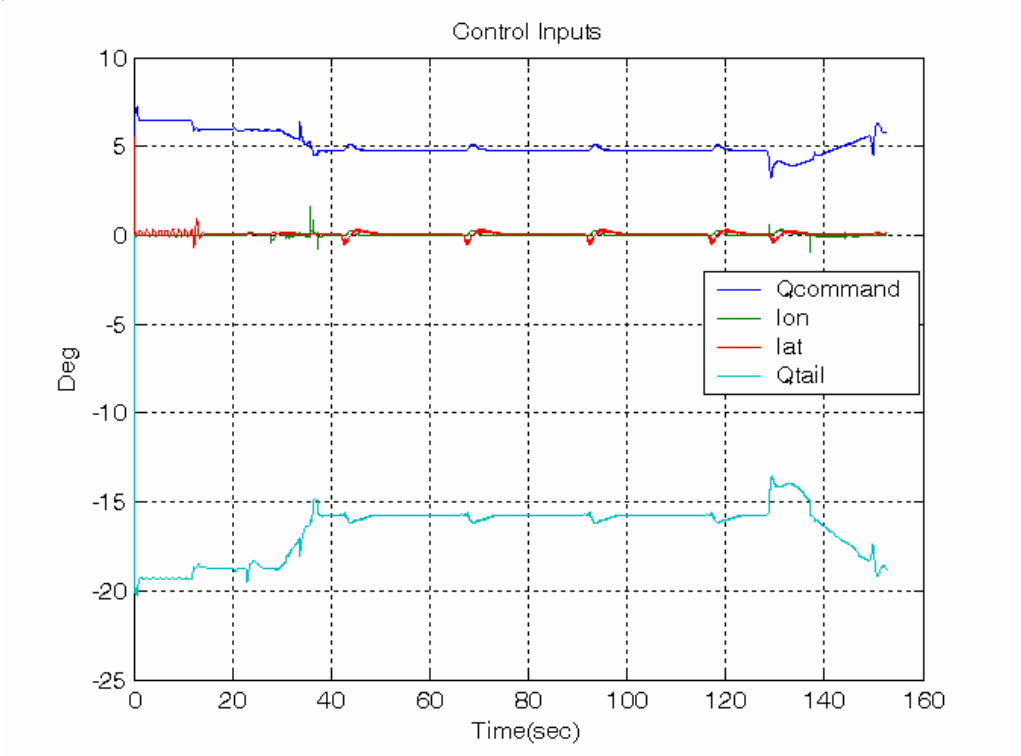

Figure 7-5 Control inputs

7.1 Conclusions

From the trajectory given in Figure 7-1, the guidance makes the helicopter traverse all the waypoints. The guidance algorithm works pretty well. The first mode of the helicopter is to ascend. During this maneuver, the autopilot stabilizes the body rates and ascends. Since helicopter has unstable dynamics, the stabilization of the body rates gets time. After the stabilization, the commanded forward velocity realized by the longitudinal autopilot and the side velocity kept zero. During bank-to-turn, the body velocities are perturbed because of the coupling. However, this coupling is insignificant.

CHAPTER 8

CONCLUSIONS

In this study, the main aim is to design an autopilot and a guidance algorithm for an autonomous small-size unmanned helicopter. By autonomy, the high maneuvering capabilities of an unmanned helicopter can be exploited in very wide range of applications. Autopilot and the guidance algorithms are the fundamental structures for autonomy.

The work done in the thesis can be separated in two parts as autopilot and guidance designs. Using an autopilot, the unmanned helicopter is stabilized and get ready to be commanded. With the guidance, helicopter traces the desired path.

The mathematical model of a small-size helicopter is derived in the first place in order to understand the dynamics. The complexity of the dynamics increases the importance of the mathematical model since unreliable models may cause serious problems in real life. For this reason, a wide literature survey is conducted and a dynamic model tested with real flight-data is chosen.

Linear quadratic regulator (LQR) technique is used to design an autopilot. Hence, the linear models are extracted from nonlinear helicopter model. The linearization is based on the Taylor series expansion of the nonlinear model. The expansion is utilized at the equilibrium point in order to cancel residual parts. The trimming is implemented for finding the equilibrium points. The linear models extracted from the nonlinear model at trim points are used to design full-state feedback by LQR. To have a global controller a synthesis of linear controllers designed by LQR at various trim points, which cover the flight envelope, is used. The gain scheduling is fulfilled in this synthesis successfully. Promising results are obtained from the simulations.

Waypoint guidance is used for guidance. Waypoints are defined by their positions and the desired velocities at the waypoints. Sequences of waypoints are used for tracking a path. The active waypoint is used by the guidance as a target position. The next waypoint is activated when the previous waypoint is reached and the sequence will end up with a trajectory. The guidance commands are generated for horizontal and vertical planes. In the horizontal plane, the line-of-sight is used as a heading command. In the vertical plane, the direction of the velocity vector is aligned with the flight path angle. The altitude rate controller is switched to the altitude controller if the altitudes of the successive waypoints are same.

The performances of the guidance and the autopilot are evaluated with a test scenario. From the results, the guidance and autopilot algorithms have sufficient performance to handle moderate maneuvers.

As a future work, harsh control algorithms can be designed to handle aggressive maneuvers. In addition, guidance algorithm may be improved to react to the changing environment such as obstacle avoidance.

REFERENCES

[1] Padfileld, G.D., *Helicopter Flight Dynamics: The Theory and Application of Flying Qualities and Simulation Modeling*, AIAA, Washington, 1996

[2] Civita La, M., "Control for Full-Envolope Flight of Robotic Helicopters", Ph.D. Thesis, Carneige Mellon University, Pittsburgh, Dec. 2002

[3] Munzinger, C., "Development of A Real-Time Flight Simulator For an Experimental Model Helicopter", M.S.Thesis, Georgia Institute of Technology, Atlanta, Dec. 1998

[4] Gavrilets, V., "Autonomous Aerobatic Maneuvering of Miniature Helicopters," Ph.D. Thesis, Massachusetts Institute of Technology, May 2003

[5] Mettler, B., "Modeling Small-Scale Unmanned Rotorcraft for Advanced Flight Control Design", Ph.D. Thesis, Carnegie Mellon University, Pittsburgh, Pennsylvania, Jan 2001

[6] McLean, D., *Automatic Flight Control Systems*, Prentice Hall International (UK) Ltd., 1990

[7] Brian L. Stevens, Frank L., Lewis, *Aircraft Control and Simulation*, John Wiley & Sons Inc., 1992

[8] Lou, C.C., Kung C.C., Chang, P.W., Yang, C.D., Chang Y.H., "Linear Helicopter Model for Global Flight Envelope Control", Journal of CCIT. vol.32, no.1, Nov. 2003

[9] La Civita, M., Messner, W. C., Kanade T.,"Modelling of Small-Scale Helicopters with Integrated First-Principles and System-Identification Techniques", American Helicopter Society 58th Annual Forum, Montreal, Canada, June 2002

[10] Mettler, B., Gavrilets, V., Feron, E., Kanade T.,"Dynamic Compensation for High-Bandwidth Control of Small-Scale Helicopter", San Francisco, CA, American Helicopter Society Specialist Meeting, January 2002

[11] Whang, H. I., Hwang, W.T., "Horizontal Waypoint Guidance Design Using Optimal Control", IEEE Transactions on Aerospace and Electronic Systems,Vol.38, No.3, pp.1116-1120,2002

[12] Bakaric, V., Vukic, Z., Antonic, R.,"Improved Basic Planar Algorithm Of Vehicle Guidance Through Waypoints By The Line Of Sight", Control, Communications and Signal Processing, 2004

[13] Thomson, D.G., Bradley, R.,"The principles and practical application of helicopter inverse simulation", Simulation Practice and Theory, Vol. 6, pp. 47-70, 1998

[14] Gavrilets, V., Mettler, B., Feron, E.,"Nonlinear Model for a Small-Size Acrobatic Helicopter", AIAA Guidance, Navigation, and Control Conference and Exhibit, Canada, 2001

[15] Kannan, S., K., Johnson N., E.,"Adaptive Trajectory Based Control for Autonomous Helicopters", Digital Avionics Systems Conference Proc., Vol. 2, pp. 8D1-1 – 8D1-12, 2002

[16] Healey, A.J., Lienard, D.,"Multivariable Sliding Mode Control for Autonomous Diving and Steering for Unmanned Underwater Vehicles", IEEE J. of Oceanic Eng. Vol.18, No. 3, pp.327-339,1993

[17] Vaneck, W.T.,"Fuzzy Guidance Controller for an Autonomous Boat", IEEE Control Sys. Mag., Vol. 17, No.2, pp. 43-51, 1997

[18] Anderson, D.J.,"Introduction to Flight", McGraw-Hill Inc., 1989

[19] Kim, K.S.”Modelling, Identification, and Trajectory Planning For A Model-Scale Helicopter”, Ph.D. Thesis, The University of Michigan, 2001

[20] Shim, H.”Hierarchical Flight Control System Synthesis for Rotorcraft-based Unmanned Aerial Vehicles”, Ph.D. Thesis, University of California, Berkeley, 2000

[21] Lee, S.”Neural Network Based Adaptive Control and Its Applications to Aerial Vehicles”, Ph.D. Thesis, Georgia Institute of Technology, 2001

[22] Musick, H.S.,”PROFGEN-A Computer Program for Generating flight Profiles”, Reference Systems Branch Reconnaissance and Weapon Delivery Division, Technical Report, 1976

[23] Rugh, W.J. “Analytical Framework for Gain Scheduling”, IEEE Control System Magazine, Vol. 11, No. 1, pp. 79-84, 1991

[24] Rugh, W.J, Shamma, J.S,”Research on gain scheduling”, Automatica, Vol. 36, No. 10, pp.1401-1425